DØ Internal Note
DØ note 3554
February 9, 1999

Method to Test the Jet Energy Scale Using Transverse Momentum Balance

Levan Babukhadia[1]
V. Daniel Elvira[2]
The University of Arizona, Tucson, Arizona 85721 [1]
State University of New York, Stony Brook, New York 11794 [2]

February 9, 1999

Abstract

This note presents a method to test the jet energy scale correction (JES) based on photon-jet and jet-jet energy balance in the transverse plane. The goal is to be able to verify, to within the uncertainty inherent in the test, current and future versions of the JES correction and error. This method could eventually be used to perform an absolute global calibration of jets, although it was not designed for that purpose. This alternative, however, would be possible at the cost of losing information about the individual uncertainties and correlations associated with the JES subcorrections.

Method to Test the Jet Energy Scale Using Transverse Momentum Balance

Levan Babukhadia[1]
V. Daniel Elvira[2]
The University of Arizona, Tucson, Arizona 85721 [1]
State University of New York, Stony Brook, New York 11794 [2]

February 9, 1999

Abstract

This note presents a method to test the jet energy scale correction (JES) based on photon-jet and jet-jet energy balance in the transverse plane. The goal is to be able to verify, to within the uncertainty inherent in the test, current and future versions of the JES correction and error. This method could eventually be used to perform an absolute global calibration of jets, although it was not designed for that purpose. This alternative, however, would be possible at the cost of losing information about the individual uncertainties and correlations associated with the JES subcorrections.

1 Motivation

The determination of the jet energy scale (JES) at DØ has not been a trivial exercise. The lack of a central magnetic field and the unavailability of test beam data at low energies and for a large sample of calorimeter modules did not allow an *in-situ* calibration of jets. The Monte Carlo (MC) simulation of the calorimeters does not mimic the jet energy response and resolution to within an uncertainty that suits the needs of many physics analyses. The jet energy calibration was, therefore, not derived from a MC tuned to the data, but mostly from collider data itself using different methods [1]. The calibration factor was divided into different subcorrections: offset (underlying event and noise), response (derived using the missing E_T projection fraction method), and showering (derived from collider data and the Herwig particle level MC).

The development of a test to verify the accuracy of the JES correction has always been a goal of the JES group. The MC closure studies performed in the past offer only a partial test given the limitations of the MC. Recent studies using Geant MC suggest that the showering loss may be larger than previously believed [2]. They also suggest the possibility of a bias in the missing E_T projection fraction method. The availability of a test to verify the JES correction becomes crucial at this point in order to verify corrections and errors.

This note presents a method to test the jet energy scale correction (JES) based on photon-jet and jet-jet energy balance in the transverse plane. The goal is to be able to verify, to within the uncertainty inherent in the test, current and future versions of the JES correction and error. This method could eventually be used to perform an absolute global calibration of jets, although it was not designed for that purpose. This alternative, however, would be possible at the cost of losing information about the individual uncertainties and correlations associated with the JES subcorrections.

2 Method

Suppose that in a collider event along with the reconstructed jet, whose energy calibration we would like to examine, there is a calorimeter object present whose energy is well measured. Then the transverse momentum[1] balance between this well-measured energy cluster and the jet can be directly employed to test the energy calibration of the latter. Since the energy scale for electromagnetic (EM) objects (such as electrons and photons) showering entirely in the EM sections of the DØ calorimeters is very accurately determined from the Z, J/ψ, and π^0 data samples [3], the large p_T direct photon production at the Tevatron in the events with exactly one photon and one jet would be an example of such events, with the photon in the role of a well-calibrated calorimeter object.

In real life, however, it is hardly possible to obtain such ideal reconstructed events—usually there are more objects present in the calorimeters as a result of next-to-leading or even higher order processes. While we still would like to select events with two *leading* (i.e. highest E_T) objects, one of which is well calibrated, in order to significantly improve statistics and make the test of the E_T balance more precise, we generalize to include the lower E_T clusters in the following way. In the *transverse* plane we introduce a unit vector $\hat{\vec{n}}$ in the direction of the well-measured energy deposit. The line perpendicular to $\hat{\vec{n}}$ divides the transverse plane into two halfplanes and all objects in the event can be classified as belonging to either of them. For each of the halfplanes we calculate the total E_T projection of all objects in that halfplane onto the direction $\hat{\vec{n}}$. Finally we calculate the ratio $\mathcal{R}$ of the total E_T projection from the halfplane *not* containing a well-calibrated calorimeter object to that from the other halfplane. Mathematically $\mathcal{R}$ can be written as:

$$\mathcal{R} = \frac{\sum\limits_{(\vec{E}_T^i \cdot \hat{\vec{n}})<0} |(\vec{E}_T^i \cdot \hat{\vec{n}})|}{\sum\limits_{(\vec{E}_T^i \cdot \hat{\vec{n}})>0} (\vec{E}_T^i \cdot \hat{\vec{n}})}, \tag{1}$$

where $(\vec{E}_T^i \cdot \hat{\vec{n}})$ is a scalar product of the two vectors. One would like to study $\mathcal{R}$ as a function of the energy and the pseudorapidity of the reconstructed jet under consideration. The closeness of such a ratio $\mathcal{R}$ to unity can be a measure of the correctness of the jet energy scale.

As mentioned earlier, the photon-jet (γ-jet) data provides us with a very good sample for testing the JES for relatively low E_T jets using $\mathcal{R}$ in Eq. 1. Unfortunately, we quickly run out of statistics in the γ-jet sample as we go to the forward regions of the detector because the γ-jet cross section at the Tevatron is smaller by three orders of magnitude than that of the dijet production, and because it also falls rather steeply with both E_T and pseudorapidity. Therefore, we use the γ-jet data to test the JES primarily in the central region, where the jet-jet data do not help. Once we establish that the jets in the central region are well calibrated, we then move to the jet-jet data sample, where we request that one of the two leading jets be central and the other one be forward. In the jet-jet data we then test the JES of the forward jet against that of the central jet (that is, the central jet now plays the role of a well-calibrated energy cluster for the purpose of constructing Eq. 1) with increased statistics for the energy

[1] All calorimeter objects are considered to be massless, hence throughout this note we use transverse *momentum* ($\vec{p}_T$) and transverse *energy* ($\vec{E}_T$) interchangeably.

and the pseudorapidity coverage of interest. The γ-jet data is also used in the forward regions to verify the jet-jet results in the kinematic range both samples overlap.

We note that the generalized $\mathcal{R}$ which includes all reconstructed calorimeter objects for estimating the E_T balance in the event is, by definition, sensitive to the unclustered energy (UCE) of the event, which results from the Reco E_T thresholds for reconstructing the calorimeter objects, most notable of which is the E_T threshold of 8 GeV in the standard DØ cone jet finder [4]. Therefore, the effect of the UCE must be estimated and removed prior to interpreting $\mathcal{R}$ of Eq. 1 as a measure of the E_T balance of the event.

In addition, depending on the physics of the event, $\mathcal{R}$ may test the E_T balance at either *parton* or *particle* level. In the γ-jet data the photon energy is fully contained and the photon should directly balance the final state hard parton. Thus the E_T balance between the leading photon and jet tests the JES to the parton level whereas in the jet-jet sample the E_T balance between the two leading jets is the test at the particle level. There is a possible loss of energy when going from parton to particle level jets due to the clustering algorithms applied for the jet finding at each level. However, the purpose of the DØ JES is to correct calorimeter jets to only *particle* level jets. Therefore, when drawing conclusions from the E_T balance studies in the γ-jet data regarding the JES, one needs to examine and take into consideration parton to particle energy difference for the jets.

Finally, studying $\mathcal{R}$ as a function of energy is challenging too. This is because binning the distributions of $\mathcal{R}$ in terms of the energy of the forward jet may bias the ratio due to the combined effect of the finite jet energy resolutions in the calorimeters and the steeply falling jet production cross section. Consider the jet-jet sample with the central and the forward leading jets and suppose we bin $\mathcal{R}$ in terms of the forward jet energy. Then, in a given energy bin, we will have more of the lower *particle* level energy jets which have fluctuated high due to the energy smearing than the higher *particle* level energy jets which have fluctuated low. However, we have made no constraint on the energy of the corresponding central jet in the event—the jet energy smearing is completely uncorrelated from jet to jet. As a result the ratio $\mathcal{R}$ of Eq. 1 will be biased towards the higher values. Therefore one needs to find an unbiased estimator of the forward jet energy and use it instead.

Based on the E_T balance method we first study the JES in the γ-jet data followed by the analysis of the jet-jet data. The issues outlined above and their solutions are discussed in great depth.

3 Photon-Jet P_T Balance

The γ-jet data sample is obtained from the collider data collected using Run 1 direct photon triggers by applying a set of quality cuts in order to select events with well measured EM objects. These cuts are described and discussed in detail elsewhere [1]; we just note that they are not designed to give a pure sample of direct photon events but rather to give a sample of events with a well-measured calorimeter object, such as one isolated photon *or* an EM cluster. We refer to these objects as photons throughout this note. In addition, there must be at least one reconstructed jet[2] in the event and we require all jets to satisfy the standard jet quality cuts described in detail elsewhere [5]. We apply the EM energy scale to the photons and the current version of the JES (Cafix 5.1) to the jets. To avoid the poorly instrumented

[2]This study is limited to 0.7 cone jets reconstructed by standard DØ jet algorithm [4].

intercryostat region and regions with coarser granularity in the third EM calorimeter layer, we require the pseudorapidity of EM clusters to satisfy $|\eta_\gamma| < 1.0$ or $1.6 < |\eta_\gamma| < 2.5$. The events are included in the sample only if the $E_{T\gamma}$ is above the corresponding trigger threshold plus $1\sigma_\gamma$, the latter being the photon energy resolution. Despite having a successful AIDA cell restoration algorithm ACRA [6], we reject events flagged by AIDA since such events are rare. To avoid possible effects of the limited accuracy for finding and reconstructing the vertex of the primary interaction, we require the instantaneous luminosity of the event to be less than 5×10^{30} cm^{-2}s^{-1}. The probability of multiple interactions in such a low luminosity sample can however still be as high as 18%. To further eliminate possible multiple interaction events we additionally require MITOOL [7] to have a value of 1 *or* 2, which means that it is very likely that the surviving events have only single interaction. Finally we require the photon and the leading jet to be back-to-back in the transverse plane to within 20° that is $|\varphi_\gamma - \varphi_{jet}| > 160°$. In Eq. 1 now $\hat{\vec{n}}$ is in the direction of the photon and we use $\mathcal{R}_{\gamma j}$ to refer to the ratios obtained from the γ-jet data sample.

The data are subdivided into seven pseudorapidity regions according to the leading jet's η as given in Table 1. In each of these pseudorapidity regions we study the ratio $\mathcal{R}_{\gamma j}$ as a

η range	Region	η range	Region
$0.0 \le |\eta| < 0.4$	CT1	$1.6 \le |\eta| < 2.0$	FW1
$0.4 \le |\eta| < 0.8$	CT2	$2.0 \le |\eta| < 2.5$	FW2
$0.8 \le |\eta| < 1.2$	IC1	$2.5 \le |\eta| < 3.0$	FW3
$1.2 \le |\eta| < 1.6$	IC2		

Table 1: Pseudorapidity regions used in this study.

function of jet energy. However, to avoid all possible biases and smearing effects originating from the finite jet energy resolution (pointed out originally in a slightly different context in [1]) we too use variable $E' = E_{T\gamma} \cdot \cosh(\eta_{jet})$ as an unbiased estimator of the jet's energy. This is because E' is constructed from two relatively well measured quantities: photon's transverse momentum $E_{T\gamma}$ and leading jet's pseudorapidity η_{jet}. A particular choice of binning in E' is entirely driven by statistics and is therefore somewhat arbitrary.

We study distributions of $\mathcal{R}_{\gamma j}$ for every pseudorapidity region and in each E' bin. Remaining contamination that causes tails in the $\mathcal{R}_{\gamma j}$ distributions is removed by fitting the distributions to Gaussians. Fig. 1 of the Appendix is an illustration of such fits for different E' bins in the CT1 pseudorapidity region. The fitted means are taken to be best estimators of the $\mathcal{R}_{\gamma j}$ in a given E' bin, and their statistical errors are estimated in the usual way dividing the width of the Gaussian fit by the square root of the number of events in the bin. Figs. 1-2 show the fitted values of $\mathcal{R}_{\gamma j}$ along with their statistical errors as a function of E' in every pseudorapidity region. In all regions the ratios $\mathcal{R}_{\gamma j}$ are fluctuating around unity without any obvious trend and stay within a band of about 2.5%, with the exception of the lowest E' point in the IC2 and the two highest E' bins in FW3 where the deviations from the unity are larger.

We try to measure the effects of the unclustered energy (UCE) on $\mathcal{R}_{\gamma j}$. For this we obtain the $\mathcal{R}_{\gamma j}$ distributions by applying different cuts E_T^{cut} of 8, 10, and 14 GeV on the reconstructed calorimeter objects. Then we proceed by fitting $\mathcal{R}_{\gamma j}$ in E' bins to Gaussians for each of the

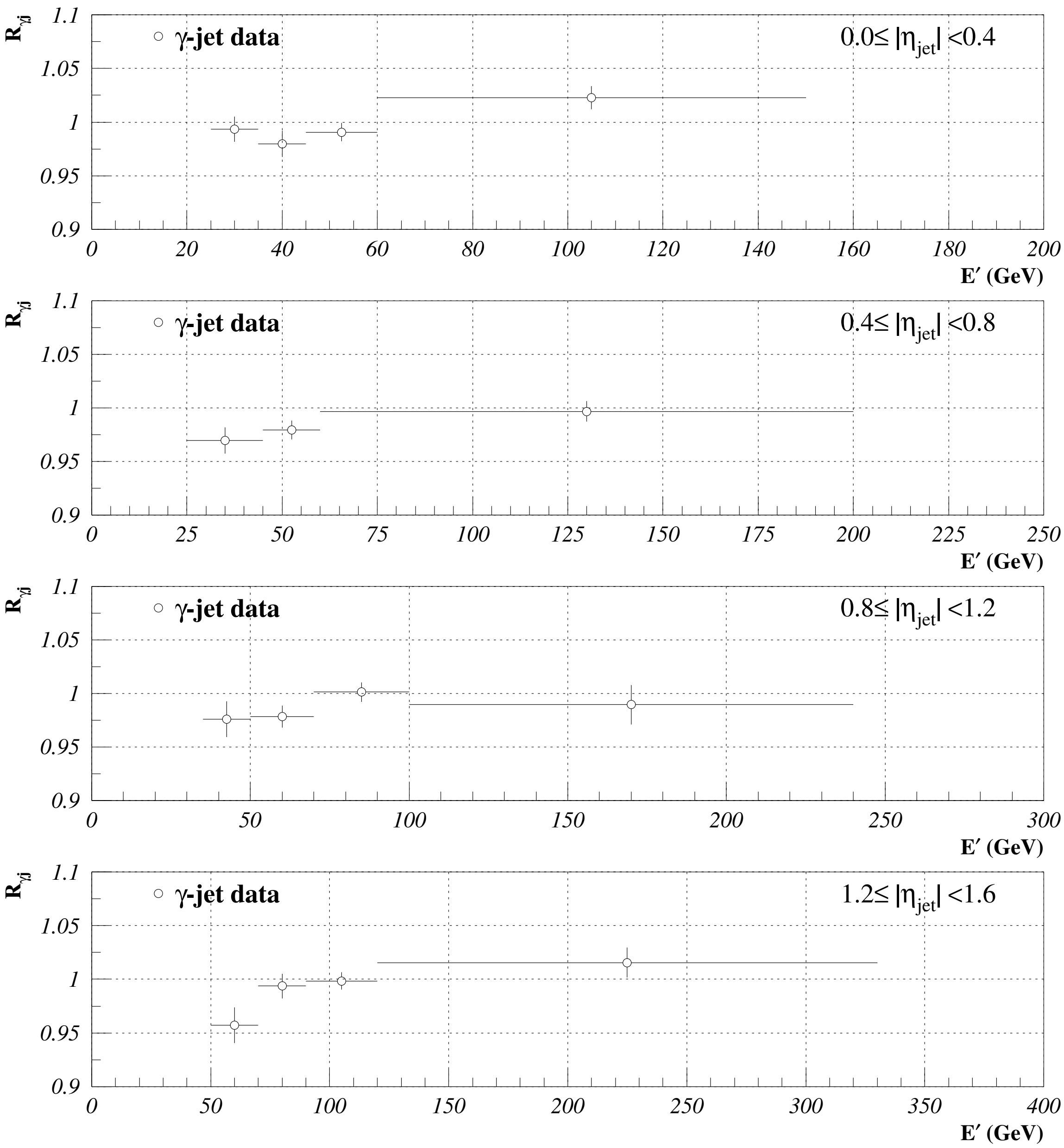

Figure 1: $\mathcal{R}_{\gamma j}$ *as a function of* E' *in central and intercryostat pseudorapidity regions.* $\mathcal{R}_{\gamma j}$ *is not corrected by the UCE or the parton to particle energy difference. The data points are plotted at the geometrical centers of the corresponding* E' *bins.*

values of the E_T^{cut}. In *each* of the E' bins the fitted mean $\mathcal{R}_{\gamma j}$ is studied as function of E_T^{cut}. Unfortunately, due to the limited statistics we are not able to extract the UCE correction in the γ-jet data, although the jet-jet results shown later in the note suggest it is different from zero and without such correction $\mathcal{R}_{\gamma j}$ would appear slightly lower than unity for low energies. For the E' bin of 70–100 GeV Fig. 2 of the Appendix gives an illustration of the Gaussian

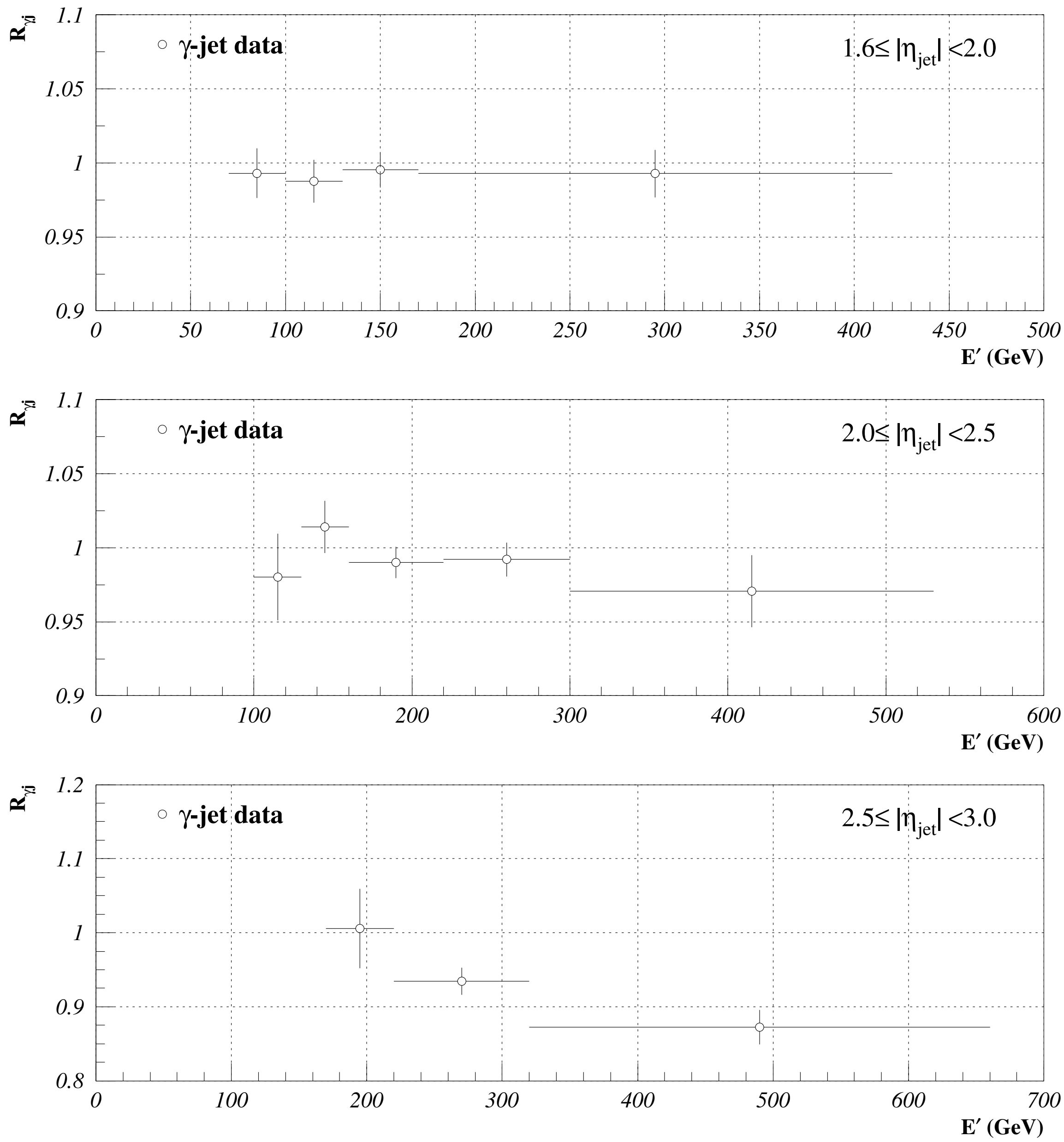

Figure 2: *$\mathcal{R}_{\gamma j}$ as a function of E' in forward pseudorapidity regions. $\mathcal{R}_{\gamma j}$ is not corrected by the UCE or the parton to particle energy difference. The data points are plotted at the geometrical centers of the corresponding E' bins.*

fits for different values of E_T^{cut}. It also shows $\mathcal{R}_{\gamma j}$ as a rather flat function of E_T^{cut} given large statistical errors on the fitted values of $\mathcal{R}_{\gamma j}$.

As mentioned earlier, the E_T balance test in case of γ-jet data is a test at the parton level rather than at the particle level. Therefore we need to examine if there are any losses in the jet momentum when going from parton to particle 0.7 cone jets. This study can only be done in the Monte Carlo (MC). Therefore we generate HERWIG MC sample and run the D0PJET algorithm to find parton and particle jets [8]. In order to avoid any effects of the UCE in the MC, we set the E_T threshold in the D0PJET algorithm to 2 GeV. The particle jets are matched up with the *closest* parton jets in the η-ϕ space. The distributions of the ratios of the transverse momenta of particle jets to that of parton jets is then fitted to Gaussians in the bins of the parton jet E_T in order to better estimate the mean of the ratio and to eliminate contamination coming from the mismatched jets. Figs. 3 and 4 of the Appendix show illustrative fits in the CT1 and FW1 regions: contamination from the mismatch shows up as a small bump at the value of the ratio of about 0.5. Bottom plots show the parton to particle jet E_T ratio as a function of the parton jet E_T. The E_T ratios are consistently below unity by about 2% on average in CT1 and by about 1.5% on average in FW1 and the deviations from unity get less with increasing parton E_T. Finally, we check how much these results are affected by applying a tight cut of $\Delta R = \sqrt{(\Delta\eta)^2 + (\Delta\phi)^2} < 0.05$ on the distance (in the η-ϕ space) between the matched parton and particle jets. Figs. 5 and 6 of the Appendix show the E_T ratios after applying this ΔR cut. The E_T ratios are still consistently below unity but now the deviation is slightly smaller: 1.5% on average in CT1 and $0.5 - 1\%$ on average in FW1. To summarize, the HERWIG MC simulations suggest that the particle level jets have on average $1 - 2\%$ less E_T than the corresponding parton level jets. The effect decreases with increasing E_T or increasing pseudorapidity of the jets.

With this effect in mind we therefore conclude that the γ-jet E_T balance studies indicate that the JES is correct to within $1-2\%$ up to the pseudorapidities of 2 and for the E_T covered in Figs. 1 and 2. While the FW2 region might be somewhat unclear, the FW3 region suggests that the jets lack some energy at these high pseudorapidities. Based on these γ-jet E_T balance studies we are convinced that the current version of the JES works rather well in the CT1 region. Therefore, to extend the limited E_T coverage (up to about 120 GeV) and to improve statistics available in the γ-jet data, we next turn to the dijet events where we require to have *either* of the leading jets central, while the other one is forward. Using the just-established fact that the JES for central jets is correct, we now can test the JES of the other, more forward jet.

4 Jet-Jet P_T Balance

The jet-jet events are extracted from the Run 1B data sample collected by four jet triggers: Jet_30, Jet_50, Jet_85, and Jet_Max, by applying a number of cuts. We require events with at least two jets reconstructed using the standard DØ 0.7 cone jet algorithm [4]. One of the two leading jets must be central (CEN) with $|\eta_{jet}^{CEN}| < 0.4$ and the other one can be anywhere in η (FOR). We require that the event, as well as *all* the jets in the event, pass the standard event and jet selection criteria which are discussed in detail elsewhere [5]. We apply CAFIX 5.1 to the jets. All events flagged by AIDA are excluded. For the same reasons as in the case of γ-jet data (see the previous section), we require the instantaneous luminosity to be less than 5×10^{30} cm^{-2}s^{-1} and MITOOL to be 1 or 2. Also, the two leading jets must be back-to-back in the transverse plane to within 20°, that is $|\varphi_{jet}^{FOR} - \varphi_{jet}^{CEN}| > 160°$. Finally, we note that in the end we combine the jet trigger data exclusively, switching from less restrictive trigger data to a more restrictive set when the statistics in the latter start to dominate, also requiring the triggers to be at least 95% efficient in the given kinematic region. In the light of the results

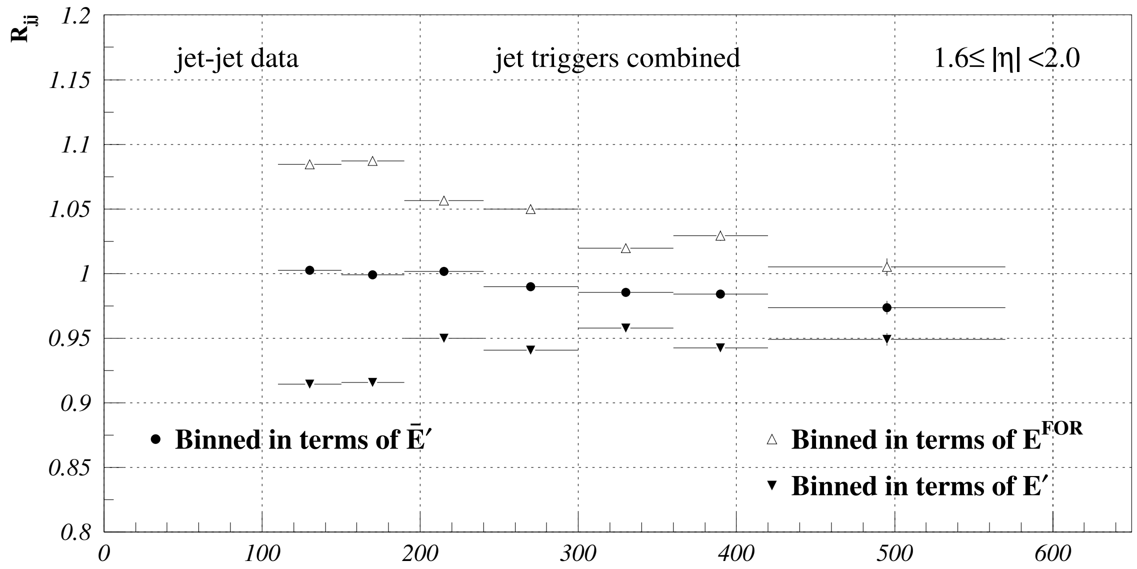

Figure 3: *Illustration of the jet E_T resolution bias on $\mathcal{R}_{jj}$from jet-jet data: when binned in terms of E^{FOR} (E') $\mathcal{R}_{jj}$ is biased high (low), but is unbiased when binned in terms of $\bar{E}'$.*

of the previous section, we now consider the central jet to represent a well-measured energy cluster and we check the JES of the other, forward jet against it. Thus, $\hat{\vec{n}}$ in Eq. 1 is now in the direction of the central jet and we use $\mathcal{R}_{jj}$ to denote total E_T projection ratios obtained from the jet-jet data.

The data are subdivided into seven pseudorapidity regions according to the *forward* leading jet's pseudorapidity η_{jet}^{FOR} using the same binning as in Table 1. We study the ratio $\mathcal{R}_{jj}$ as a function of the energy of the forward jet E^{FOR}. Experience with γ-jet data suggests that binning $\mathcal{R}_{jj}$ directly in terms of E^{FOR} may bias $\mathcal{R}_{jj}$ to the higher values due to the finite jet energy resolutions. Therefore, in addition to E^{FOR}, we consider two other variables as candidates for the unbiased estimator of E^{FOR}. In an analogy with the γ-jet studies, as the first such candidate we consider E' which now is defined by $E' = E_T^{CEN} \cdot \cosh(\eta_{jet}^{FOR})$. As the second such candidate for the unbiased estimator of the forward jet's energy we construct and consider the quantity $\bar{E}'$ defined by:

$$\bar{E}' = \frac{1}{2}(E_T^{CEN} + E_T^{FOR}) \cdot \cosh(\eta_{jet}^{FOR})\,. \qquad (2)$$

For each of the jet trigger data separately and in every η_{jet}^{FOR} region we first fit $\mathcal{R}_{jj}$ distributions to the Gaussians in the bins of these three energy-like quantities E^{FOR}, E', and $\bar{E}'$. Figs. 7–10 of the Appendix illustrate the procedure when binned in terms of $\bar{E}'$, for individual jet trigger data in the FW1 region. The fitted means are taken to represent the average $\mathcal{R}_{jj}$ in a given bin, and the statistical error is estimated dividing the width of the fitted Gaussians by the square root of the number of entries in the bin. Fig. 3 shows $\mathcal{R}_{jj}$ in the FW1 region binned in terms of the three variables under consideration. Comparing this to the γ-jet data

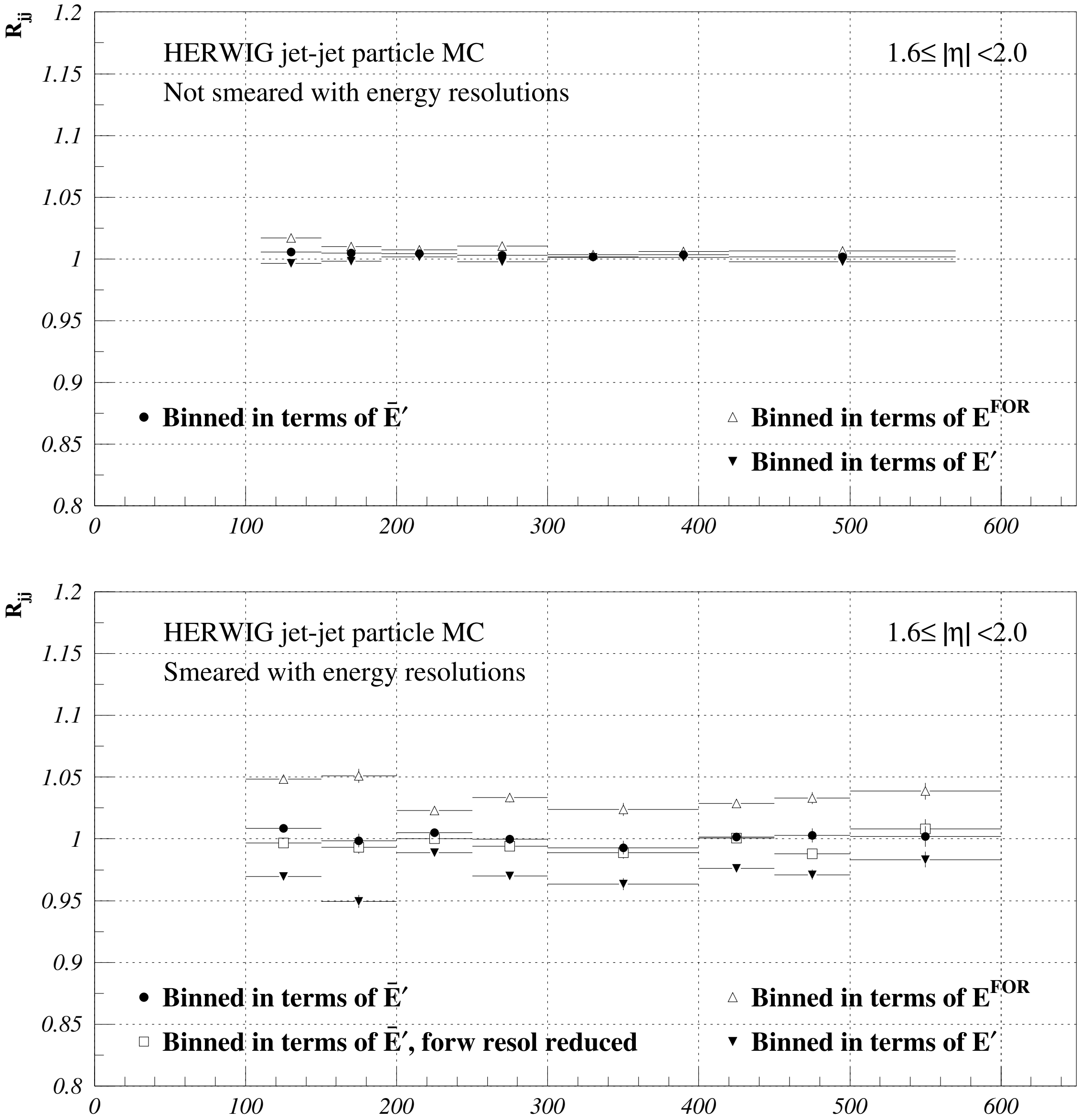

Figure 4: *The* HERWIG *particle level MC shows no bias (top plot). However, as soon as the MC particle jets are smeared by the jet energy resolutions (bottom plot), bias appears when binned in either E^{FOR} or E' but binned in $\bar{E}'$ remains unbiased. Even when the forward energy resolutions are artificially lowered by additional 20%, binning in $\bar{E}'$ stays unbiased (open squares in the bottom plot).*

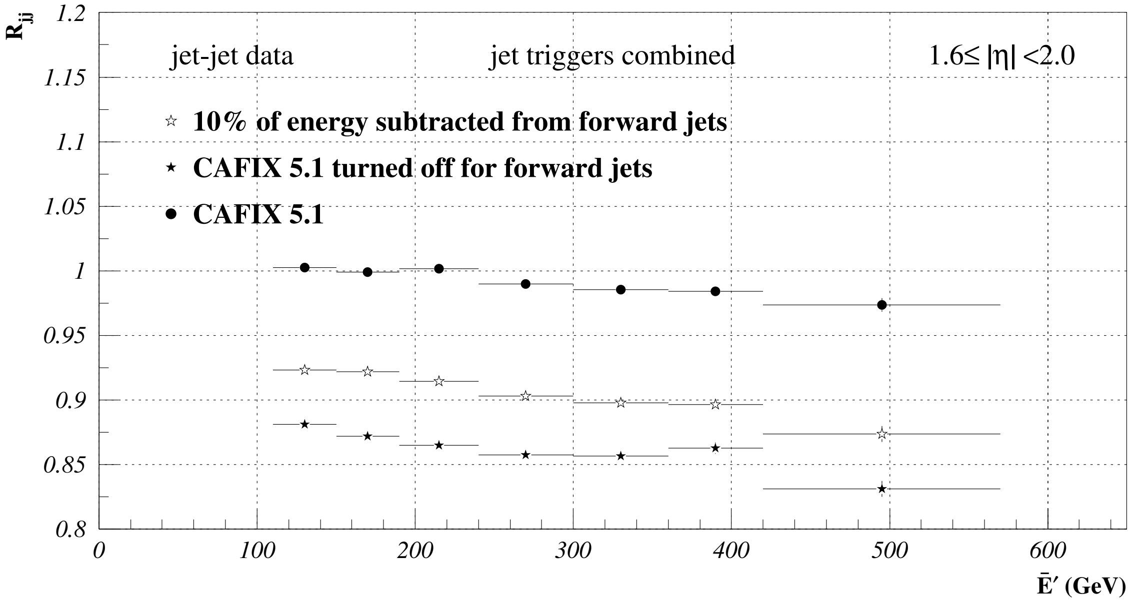

Figure 5: *Illustration of the sensitivity of the E_T balance method to the miscalibration of jets.*

in the same pseudorapidity region (top plot in Fig. 2), one concludes that the binning in terms of $\bar{E}'$ provides the most unbiased determination of $\mathcal{R}_{jj}$. The binning in terms of E^{FOR} biases $\mathcal{R}_{jj}$ high, as is expected. In addition, it is clear that the binning in terms of E' in case of the jet-jet data biases $\mathcal{R}_{jj}$ low, and therefore E' must be discarded as candidate for an unbiased estimator of the forward jet's energy. This might at first sound counter-intuitive given our experience with γ-jet data. However, one must take into consideration the fact that the photon resolution is *much* better than the jet resolution. Given poor enough jet energy resolution, the bias towards the lower values of $\mathcal{R}_{jj}$ when binned in terms of E' can be understood in the following way. In a given E' bin we have more of the lower particle energy jets which have fluctuated high due to the energy resolutions than the other way around. However, the corresponding forward jets are not subject to any requirement since the jet energy smearing is completely uncorrelated from jet to jet in a given event. This on average yields larger denominator as compared to the numerator in Eq. 1 biasing the ratio $\mathcal{R}_{jj}$ low. In fact, to the extent that jet energy resolutions are the same in the central and endcap calorimeters, this is exactly the inverse of the high bias seeing when binned in terms of E^{FOR}.

For further checks of these conclusions a dedicated HERWIG particle level MC sample was generated. Once again, in order to avoid any possible effects of the UCE in the MC, we set the E_T threshold to 2 GeV in the D0PJET algorithm. In the particle level MC there is no energy smearing except for rather small effective particle level "energy resolution" arising from the fact that there is necessarily some out of cone particle emission as soon as one uses a fixed cone algorithm for jet finding. This effect has been well understood in the course of jet energy resolution studies and in that context is often referred to as "Particle Level Dijet Imbalance" [9]-[11]. Therefore, one would expect that the results of binning in either of the

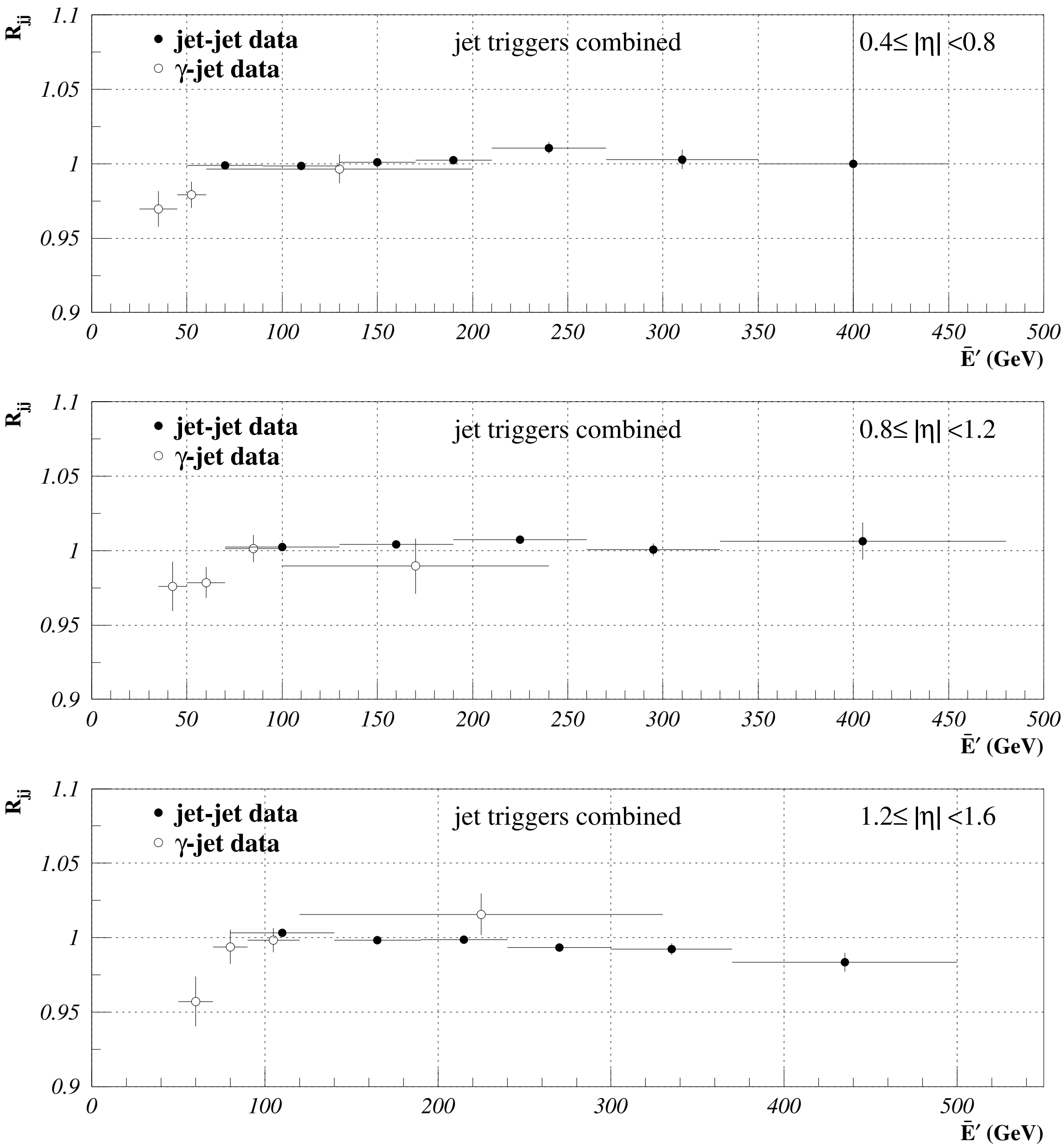

Figure 6: *$\mathcal{R}_{jj}$ as a function of $\bar{E}'$ is shown in three pseudorapidity regions. Data points from γ-jet data are overlayed for the purpose of qualitative comparison—note that the jet-jet data here is not corrected for the UCE.*

three variables would not be different. Top plot in Fig. 4 confirms this expectation. It also suggests that at the particle level *without* UCE the jets balance to within about 0.5% implying that the UCE-corrected $\mathcal{R}_{jj}$ from the jet-jet data is a measure of the jet E_T balance at the *particle* level and as such can be used to test the JES.

In addition, we smear particle level jets by the energy resolutions [9] and check if this

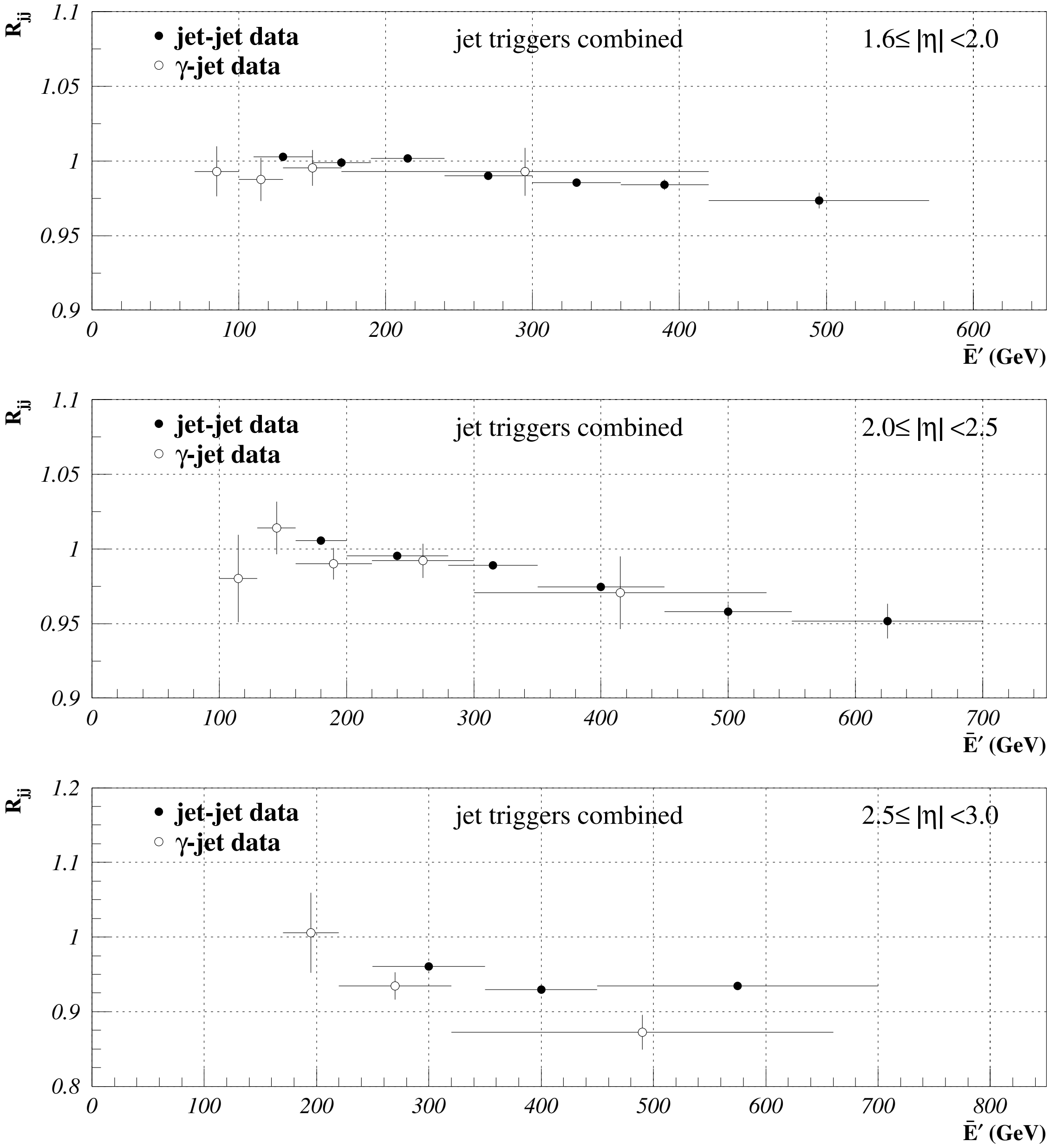

Figure 7: *$\mathcal{R}_{jj}$ as a function of $\bar{E}'$ is shown in three pseudorapidity regions. Data points from γ-jet data are overlayed for the purpose of qualitative comparison—note that the jet-jet data here is not corrected for the UCE.*

in fact introduces a bias similar to what is seen in the jet-jet data. Most recent jet energy resolutions [11] are only determined up to the jet pseudorapidity of 2. Currently the project is underway to re-derive the jet energy resolutions and extend the η coverage up to 3. Once these resolutions are available, this test can be repeated. Meanwhile, however, we note that the differences between the resolutions from [11] and [9] are within 20% of each other, and

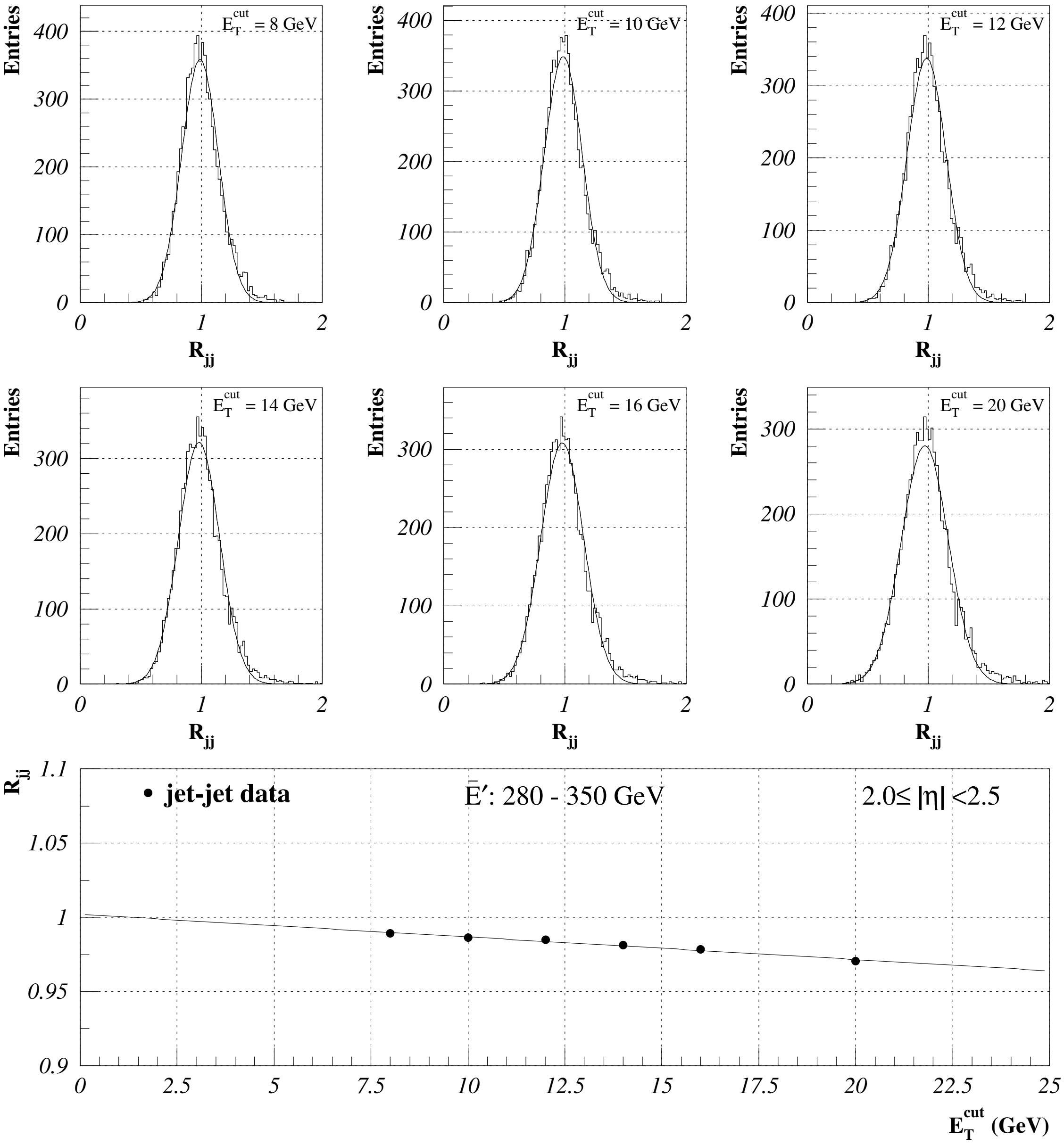

Figure 8: *Illustration of the derivation of the unclustered energy correction in jet-jet data.*

we choose to use the latter resolutions because they do extend up to the η of 3.

In the bottom plot of Fig. 4, $\mathcal{R}_{jj}$ is shown as a function of the three variables E^{FOR}, E', and $\bar{E}'$ from the MC, where now particle level jets are smeared by the jet energy resolutions from [9]. Confirming our hypothesis, the bias appears in $\mathcal{R}_{jj}$ when it is binned in terms of either E^{FOR} or E', while binned in terms of $\bar{E}'$ the ratios remain unbiased.

We stress that, as it can be seen from Figs. 3 and 4, the binning in terms of $\bar{E}'$ actually removes the E_T resolution bias to within 1%, rather than just averages the two biases seen

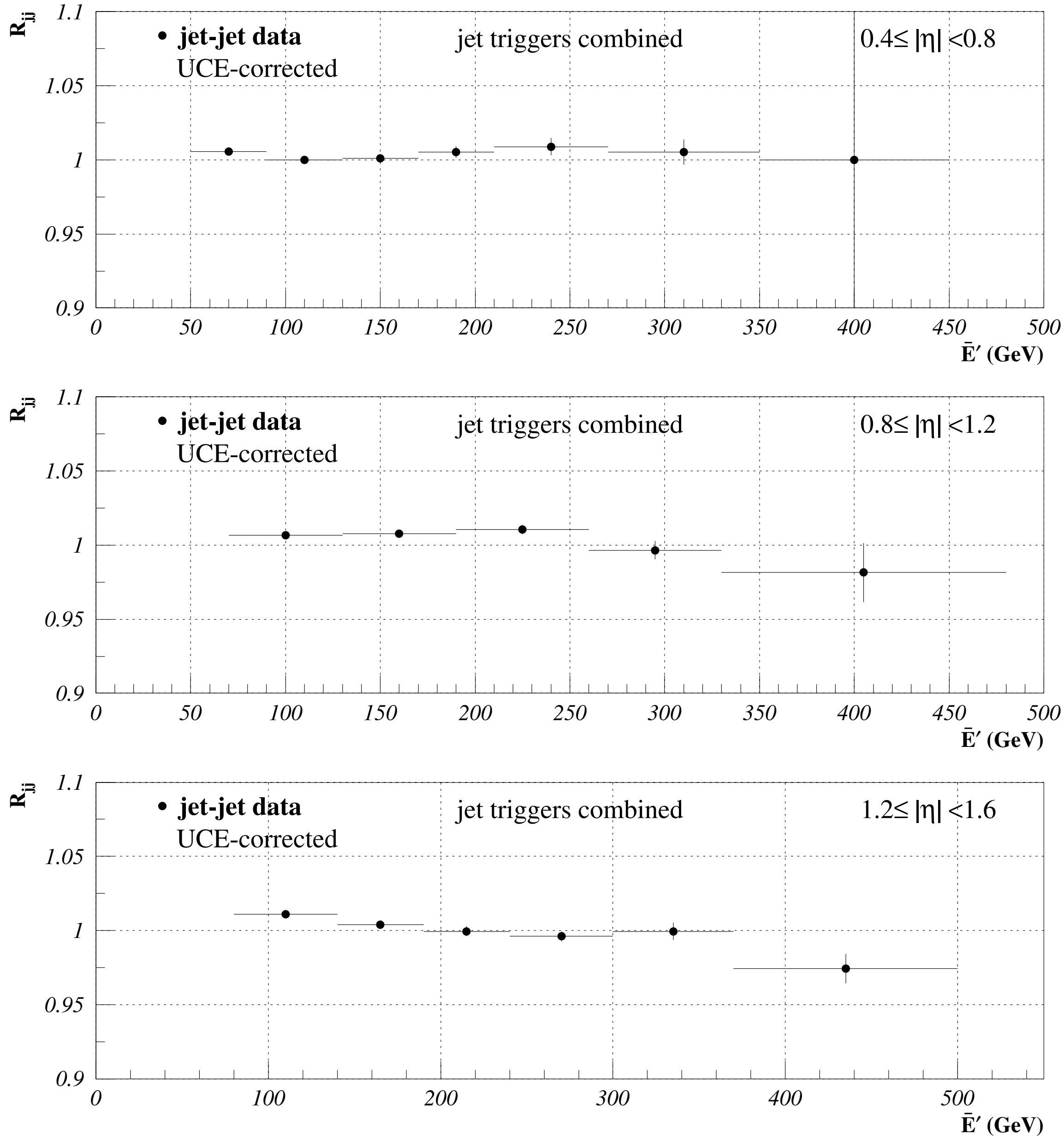

Figure 9: *$\mathcal{R}_{jj}$ as a function of $\bar{E}'$ is shown in three pseudorapidity regions after the unclustered energy correction is applied.*

when binned in terms of E^{FOR} and E'. The absence of bias in $\bar{E}'$ might be affected by the large differences between the central and forward jet energy resolutions. Based on the available resolutions, we rather conservatively estimate the difference between the central and forward resolutions to be 20%. We once again smear the MC particle level jets, but now forward jets are smeared by 20% less resolutions than what is measured in [9] and central jets are smeared by the measured central resolutions. Open squares in the bottom plot of Fig. 4 show the

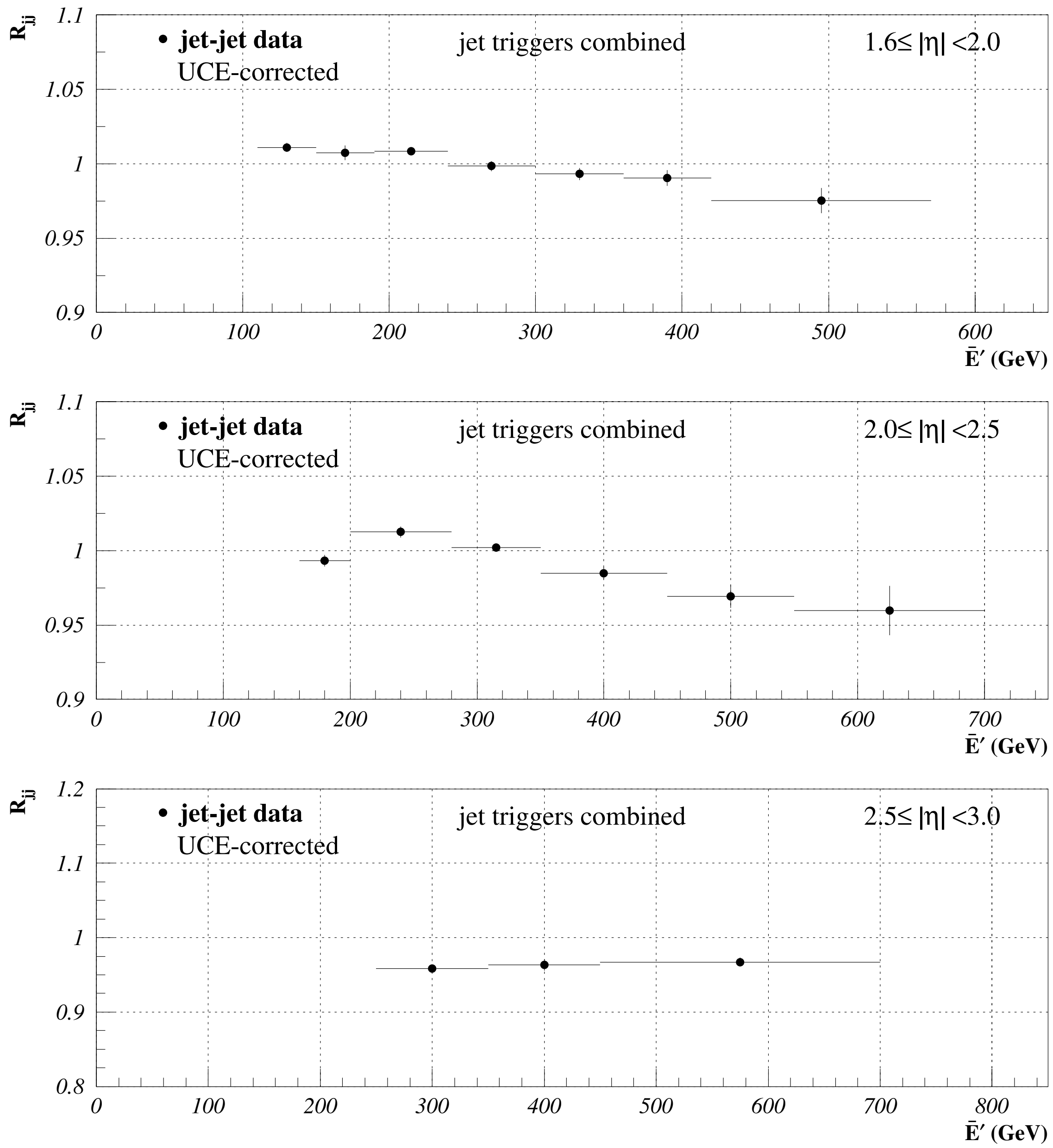

Figure 10: $\mathcal{R}_{jj}$ *as a function of* $\bar{E}'$ *is shown in three pseudorapidity regions after the unclustered energy correction is applied.*

resulting $\mathcal{R}_{jj}$ as a function of $\bar{E}'$. Once again no significant bias is observed. Based on these tests, we conclude that in the case of jet-jet data the best estimator of the forward jet's energy is $\bar{E}'$ which is free of the E_T resolution bias to within about 1%.

To check how sensitive $\mathcal{R}_{jj}$ really is to the miscalibration of jets when binned in terms of $\bar{E}'$, we did the following two tests using Run 1B data. First we completely "turned off" the JES for the forward jets and re-did everything. Next we subtracted 10% of the energy from the JES-corrected forward jets and re-did the analyses. Fig. 5 shows the results for the FW1 region. In the second case $\mathcal{R}_{jj}$ has dropped by about 8% on average while in the first case the ratios dropped by about 13% on average, which is very close to the JES correction in the FW1 region.

Having convinced ourselves that the $\mathcal{R}_{jj}$ as a function of $\bar{E}'$ is an unbiased and sensitive measure of the correctness of the JES, we next compare results from jet-jet data to those obtained earlier from γ-jet data. Figs. 6 and 7 show the results from jet-jet data overlayed with γ-jet data. While one needs to be careful when directly comparing the results of the E_T balance from γ-jet and jet-jet data (because in the former it is a test at the parton level and in the latter—at the particle level), the agreement between the two is excellent.

Finally we study the effects of the UCE on $\mathcal{R}_{jj}$. We apply 8 (default), 10, 12, 14, 16, and 20 GeV cuts (E_T^{cut}) on the *uncorrected* E_T of non-leading jets and examine $\mathcal{R}_{jj}$ as a function of E_T^{cut}. Increasing the value of E_T^{cut} results in an obvious trend of decrease of the ratio $\mathcal{R}_{jj}$ (see for example Fig. 8 in the text and Figs. 11 and 12 in the Appendix). In order to correct for the effect of the UCE, we fit a straight line to the ratios as a function of E_T^{cut}, and extrapolate the fitted function down to $E_T^{cut} = 0$. This extrapolated value of the fitted line is then taken as a UCE-corrected value for $\mathcal{R}_{jj}$. The UCE correction is derived and applied in every pseudorapidity region. The $\mathcal{R}_{jj}$ as a function of $\bar{E}'$ *after* the UCE correction is finally shown in Figs. 9 and 10. In the central and intercryostat pseudorapidity regions $\mathcal{R}_{jj}$ is consistent with unity to within about $1 - 1.5\%$, ignoring the last data points in IC1 and IC2 which have larger statistical errors and have fluctuated by about 2.5% below unity. However, in the forward pseudorapidity regions (i.e. $|\eta| > 1.6$) we start to see some deficit in the forward jet's energy. In FW1 the $\mathcal{R}_{jj}$ is consistent with unity to within about 1.5% up to the energies of 400 GeV, and drops below unity by about 2.5% near 500 GeV in energy. In FW2 deviations from unity are within 2% at and below 400 GeV and drop below unity by as much as $3 - 4\%$ for energies above 400 GeV. Finally, in FW3 we see deficiency of about $4 - 5\%$ in the forward jet's energy.

5 Conclusion

We have presented a method to test the JES based on photon-jet and jet-jet energy balance in the transverse plane. The current version of the JES, CAFIX 5.1, was verified to be correct to within its uncertainty band in the range it was investigated. Our results suggest, however, that CAFIX 5.1 systematically undercorrects jets at high pseudorapidities. The difference between the nominal ratio and unity in FW1 (FW2) pseudorapidity region grows from about 1.5% (2%) at and below 400 GeV of energy up to about 2.5% (4%) above 400 GeV; in FW3 the deviation from unity is about $4 - 5\%$ throughout the energy range covered.

References

[1] B. Abbott *et al.*, "Jet Energy Scale at DØ", DØ Note 3287.

[2] A. Goussiou, "New Showering Correction for the Jet Energy Scale at DØ", DØ Note xxxx.

[3] J. Kotcher, "Design, Performance, and Upgrade of the DØ Calorimeter", FERMILAB-CONF-95-007-E, Jan. 1995 (15). Published in the proceedings of 1994 Beijing Calorimetry Symposium, Beijing, P. R. Chian, 25–27 Oct. 1994.

U. Heintz, " A Measurement of the Calorimeter Response Using π^0 Decays", DØ Note 2268.

M. Demarteau *et al.*, " Measurement of the W Mass", DØ Note 2929.

[4] N.J. Hadley, "DØ Algorithm for Jet Finding", DØNote 904.

[5] L. Babukhadia, "Studies of Event/Jet Selection Criteria and their Efficiencies with DØ Run 1B Data", DØ Note 3373 (Talk presented at DØ QCD meeting 12 December 1997).

L. Babukhadia *et al.*, "Standard Jet Cuts and their Efficiencies for Run 1B DØ Collider Data", DØ Note 3407.

[6] G.C. Blazey, R. Hirosky, "The DØ Inclusive Cross Section", DØ Note 3276.

L. Babukhadia *et al.*, "Hot Cells and Jets at DØ (AIDA Cell Restoration)", DØ Note 3407.

[7] G. Manning *et al.*, "DØ Software Documentation", Calorimeter Reconstruction Section (1995).

[8] We would like to express our thanks to Rob Snihur who helped great deal in this effort.

[9] M. Brattacharjee *et al.*, "Jet Energy Resolutions", DØ Note 2887.

[10] I.A. Bertram *et al.*, "Single Jet Energy Resolutions at DØfor Run 1", DØ Note 3414.

[11] G.G. Di Loreto, "The Triple Differential Di-Jet Cross Section at $\sqrt{s} = 1.8$ TeV", Ph.D. thesis, Michigan State University (1998).

Appendix

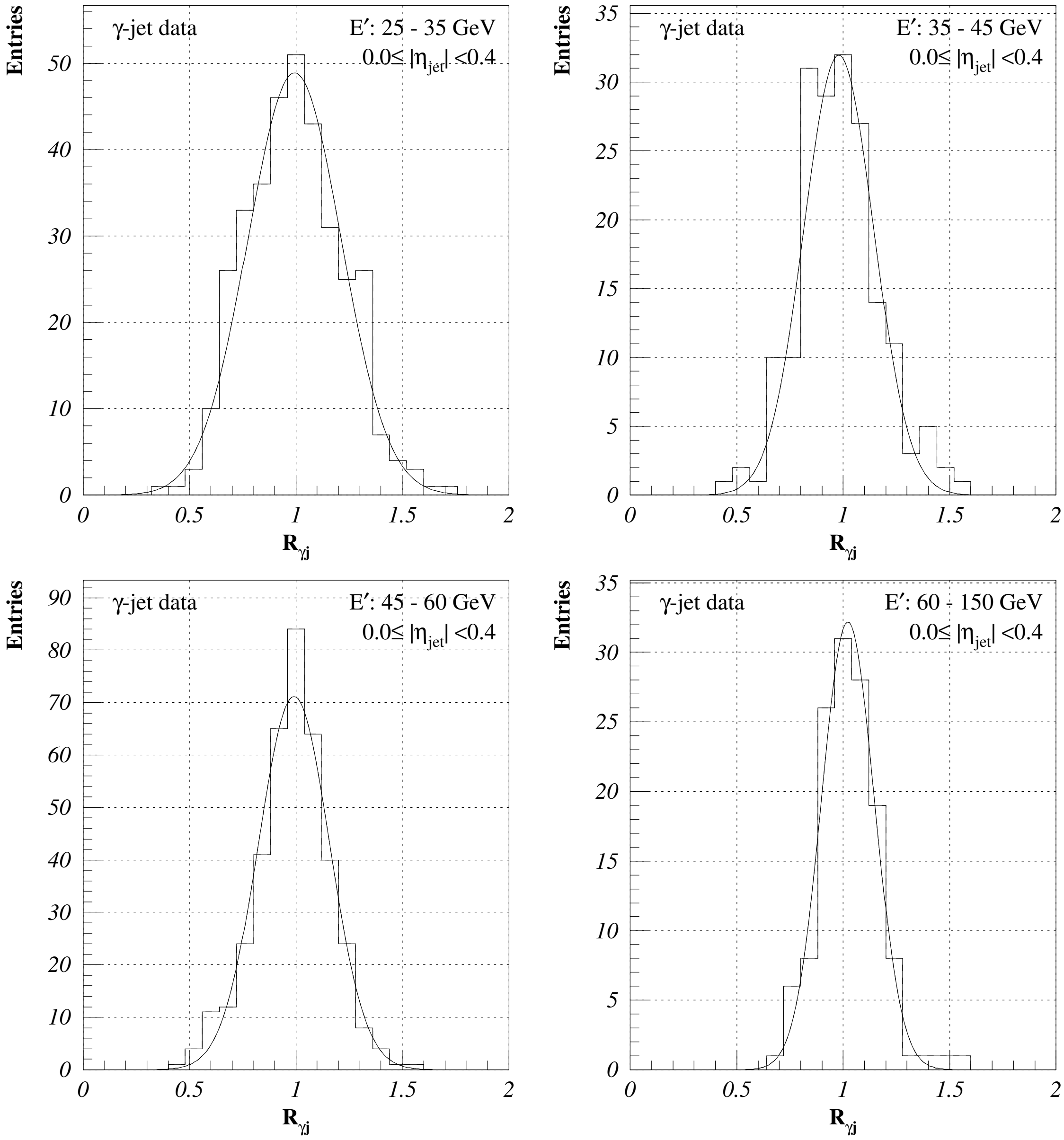

Figure 1: *Distributions of $\mathcal{R}_{\gamma j}$ are fitted to Gaussians in each of the E' bins. For illustration fits in* CT1 *region are shown here.*

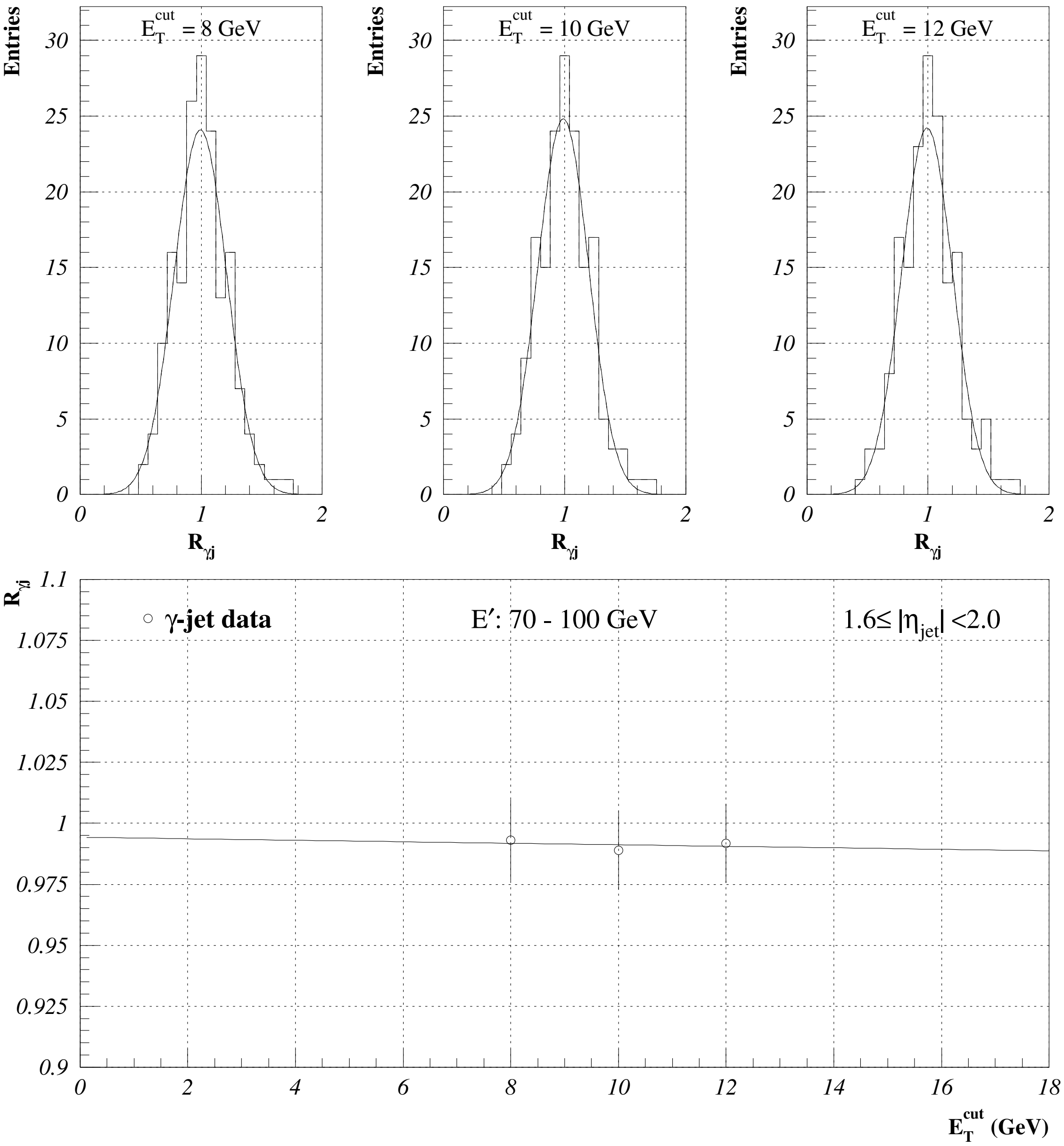

Figure 2: *Illustration of the derivation of the unclustered energy correction in γ-jet data. The bottom plot suggests that the UCE correction can not be reliably determined given the large statistical errors.*

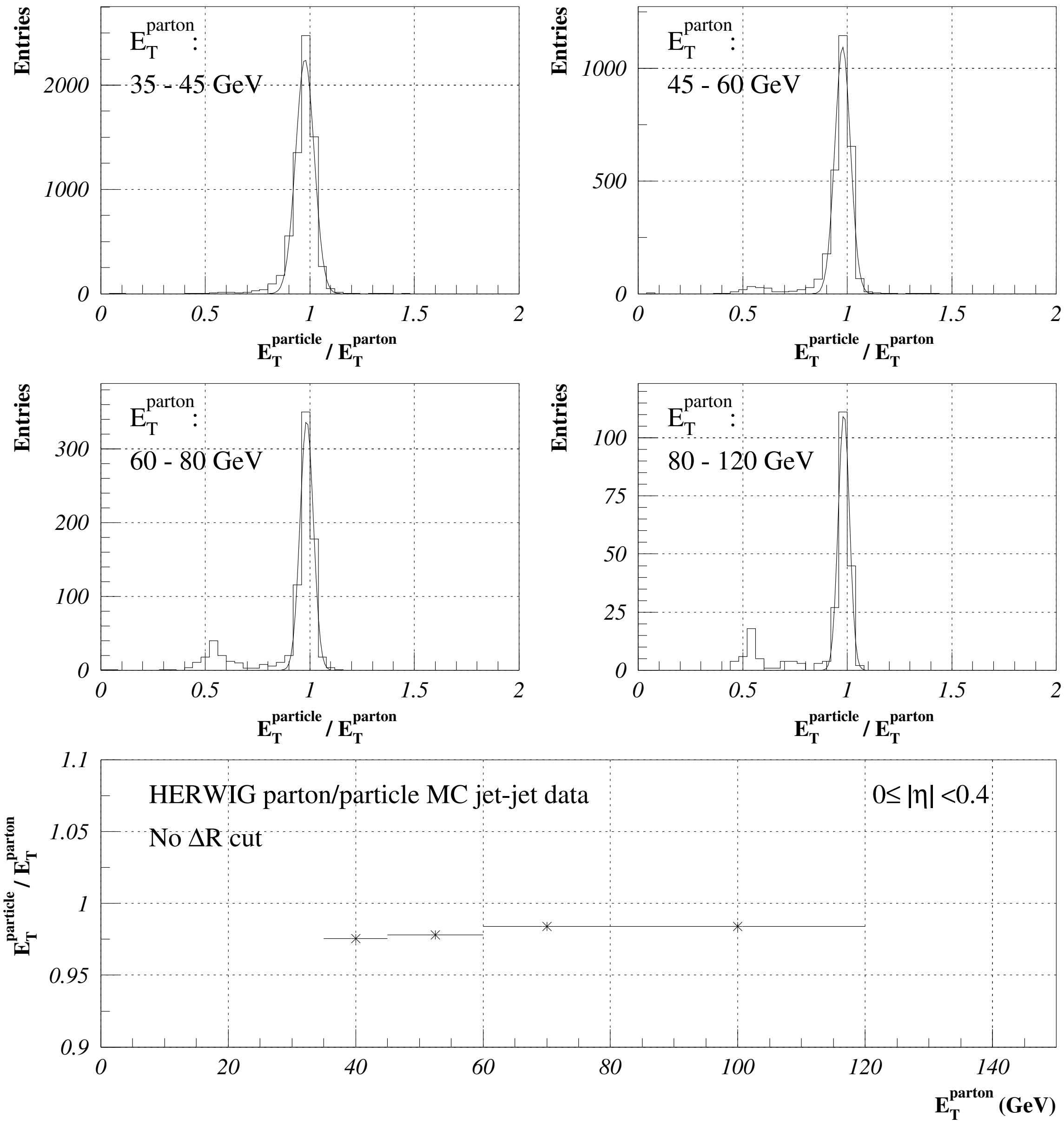

Figure 3: *The ratios of particle to parton E_T as a function of parton E_T from the* HERWIG *MC. When matching up particle jets with parton jets no cut on ΔR has been applied.*

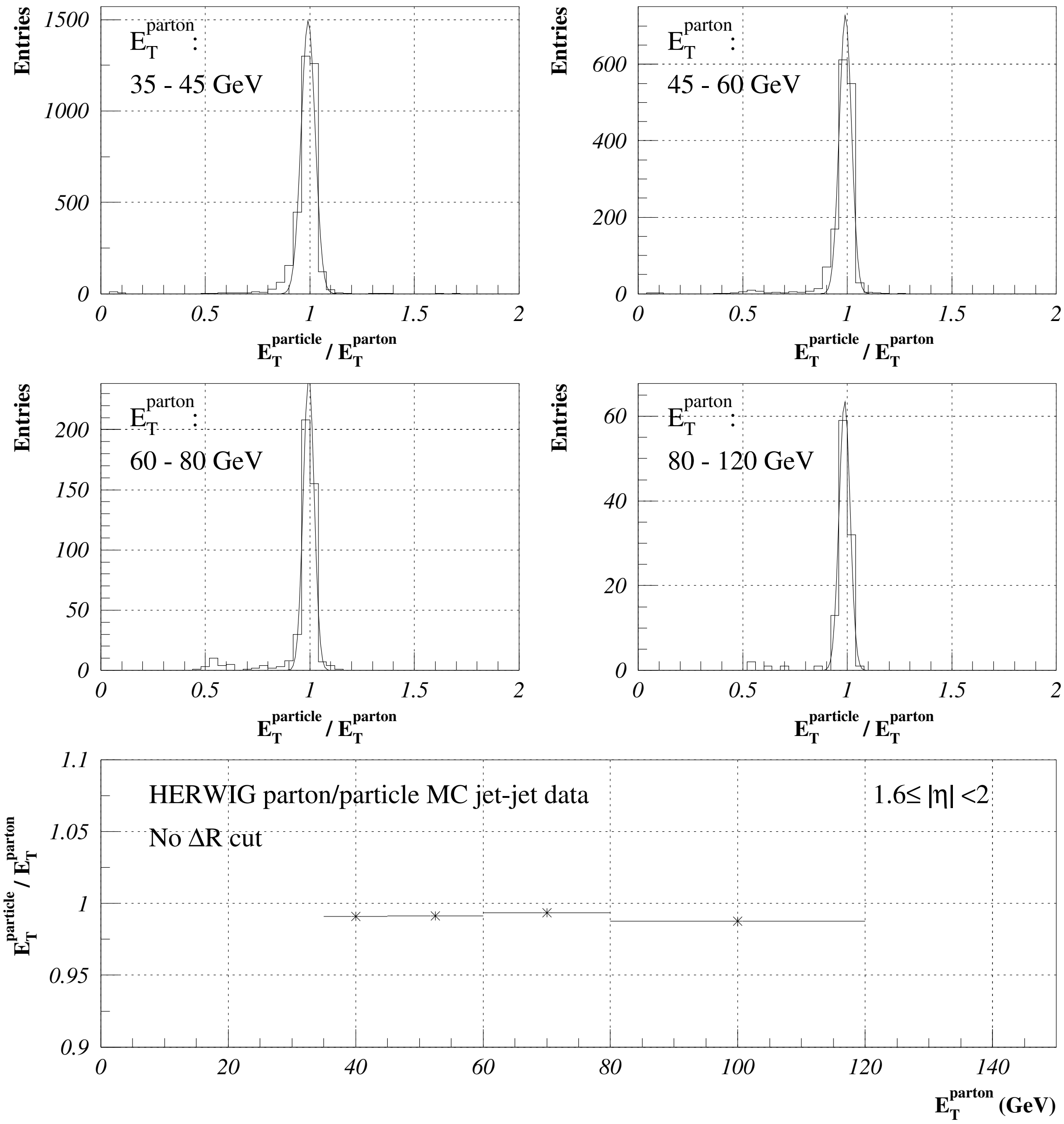

Figure 4: *The ratios of particle to parton E_T as a function of parton E_T from the* HERWIG *MC. When matching up particle jets with parton jets no cut on ΔR has been applied.*

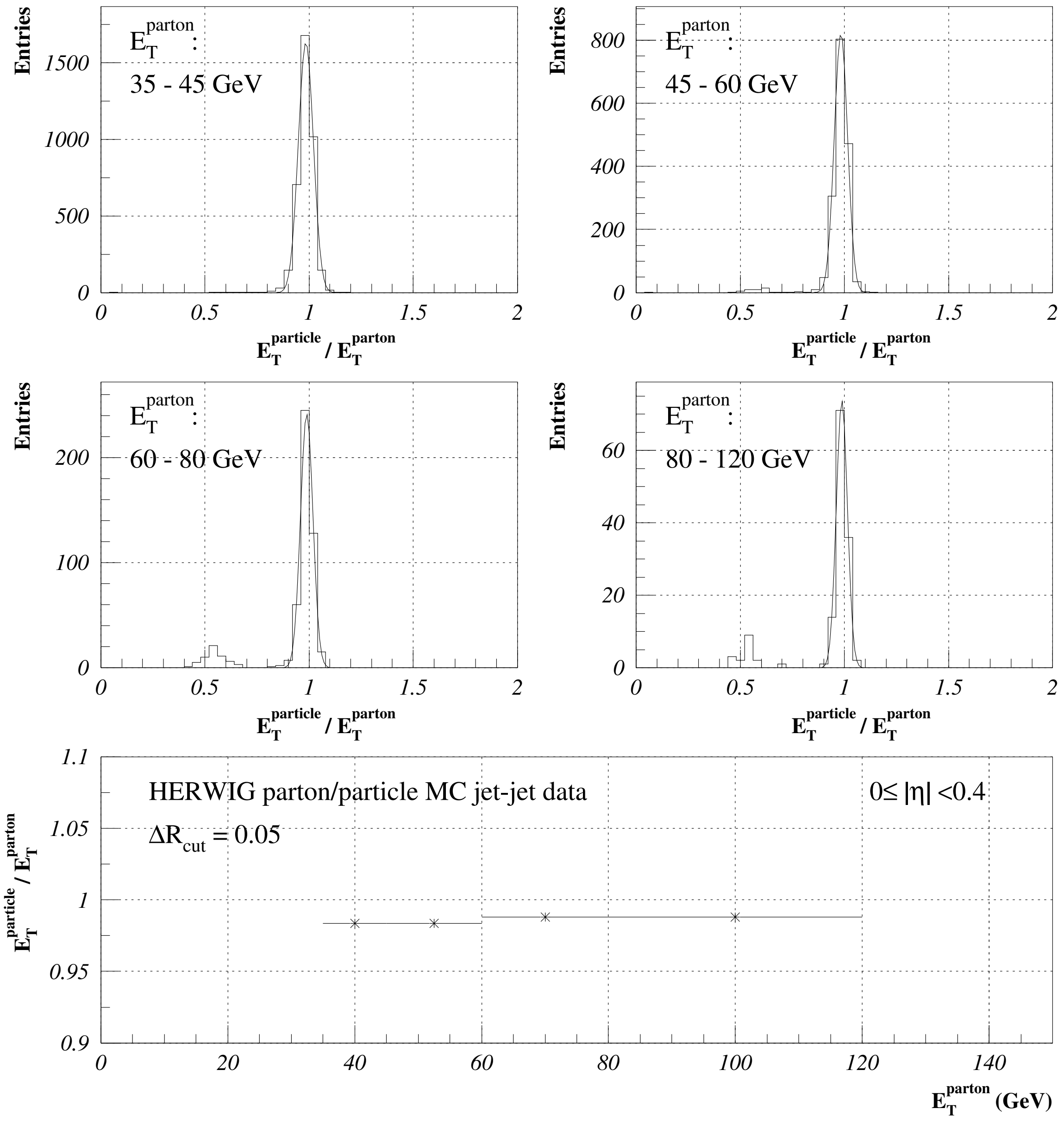

Figure 5: *The ratios of particle to parton E_T as a function of parton E_T from the* HERWIG *MC. When matching up particle jets with parton jets a cut on ΔR of* 0.05 *has been applied.*

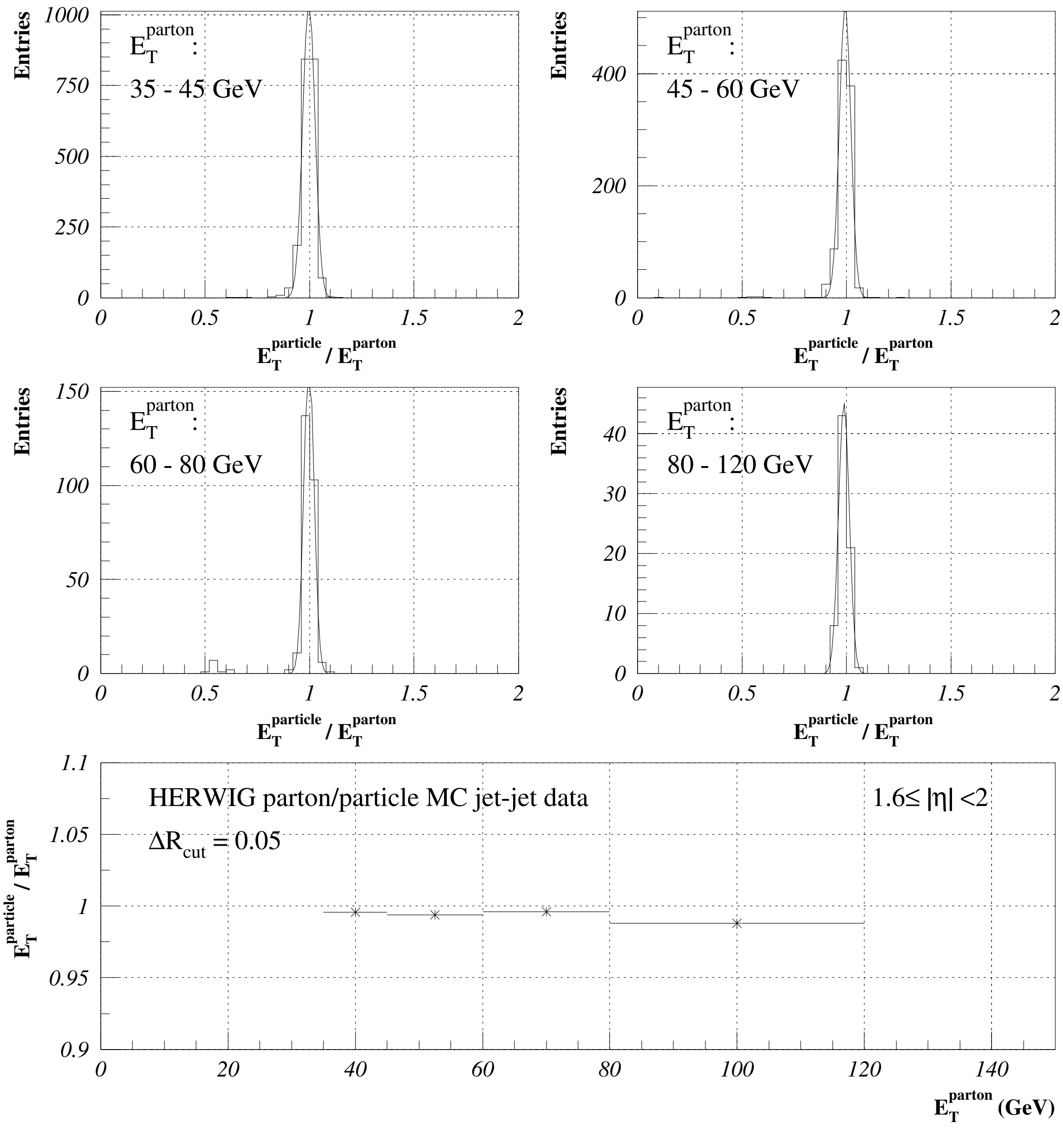

Figure 6: *The ratios of particle to parton E_T as a function of parton E_T from the* HERWIG *MC. When matching up particle jets with parton jets a cut on ΔR of* 0.05 *has been applied.*

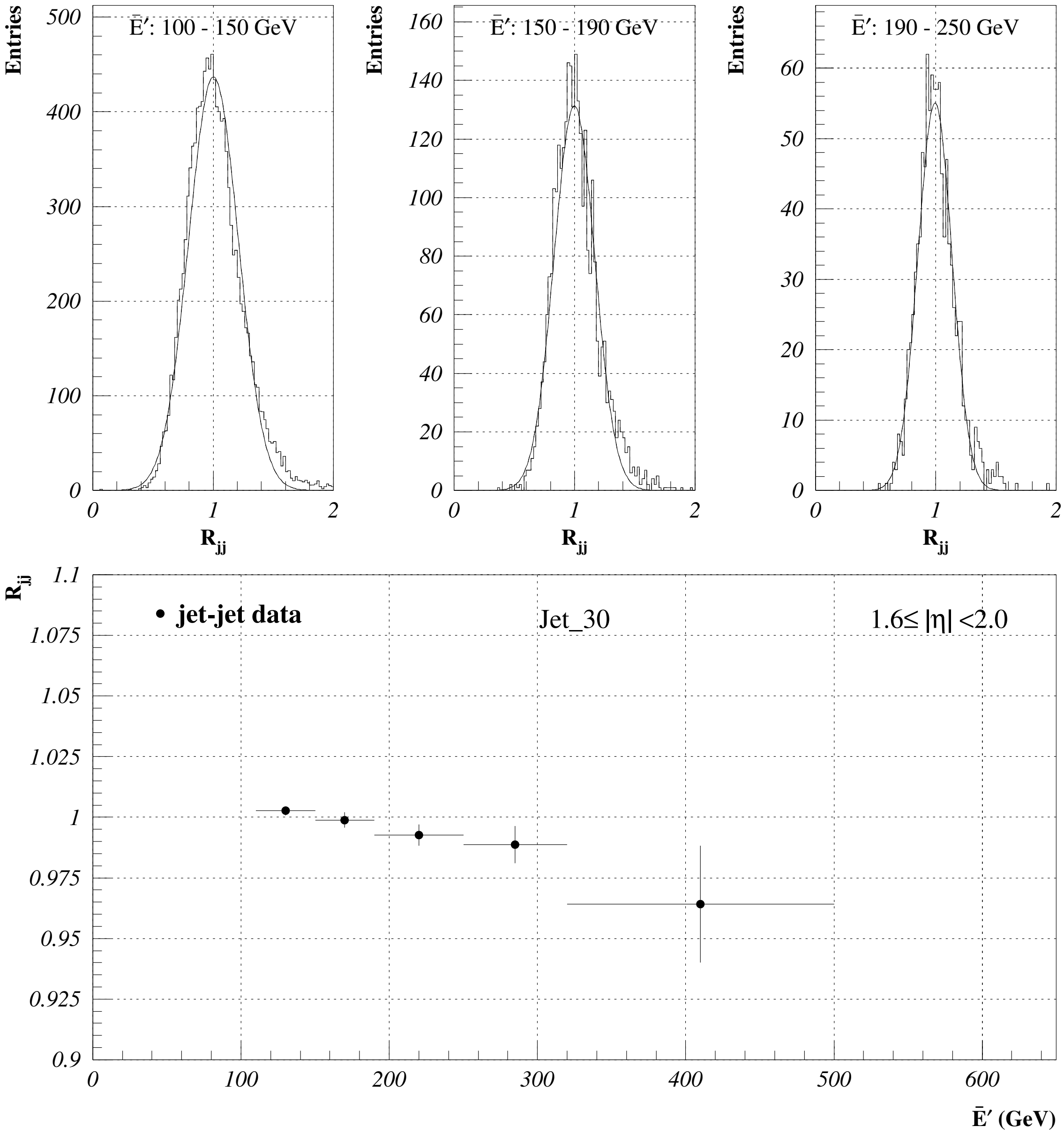

Figure 7: *Using the* Jet_30 *data the fits to Gaussians of the* $\mathcal{R}_{jj}$ *distributions in the* E' *bins with most statistical significance are shown along with* $\mathcal{R}_{jj}$ *as a function of* $\bar{E}'$.

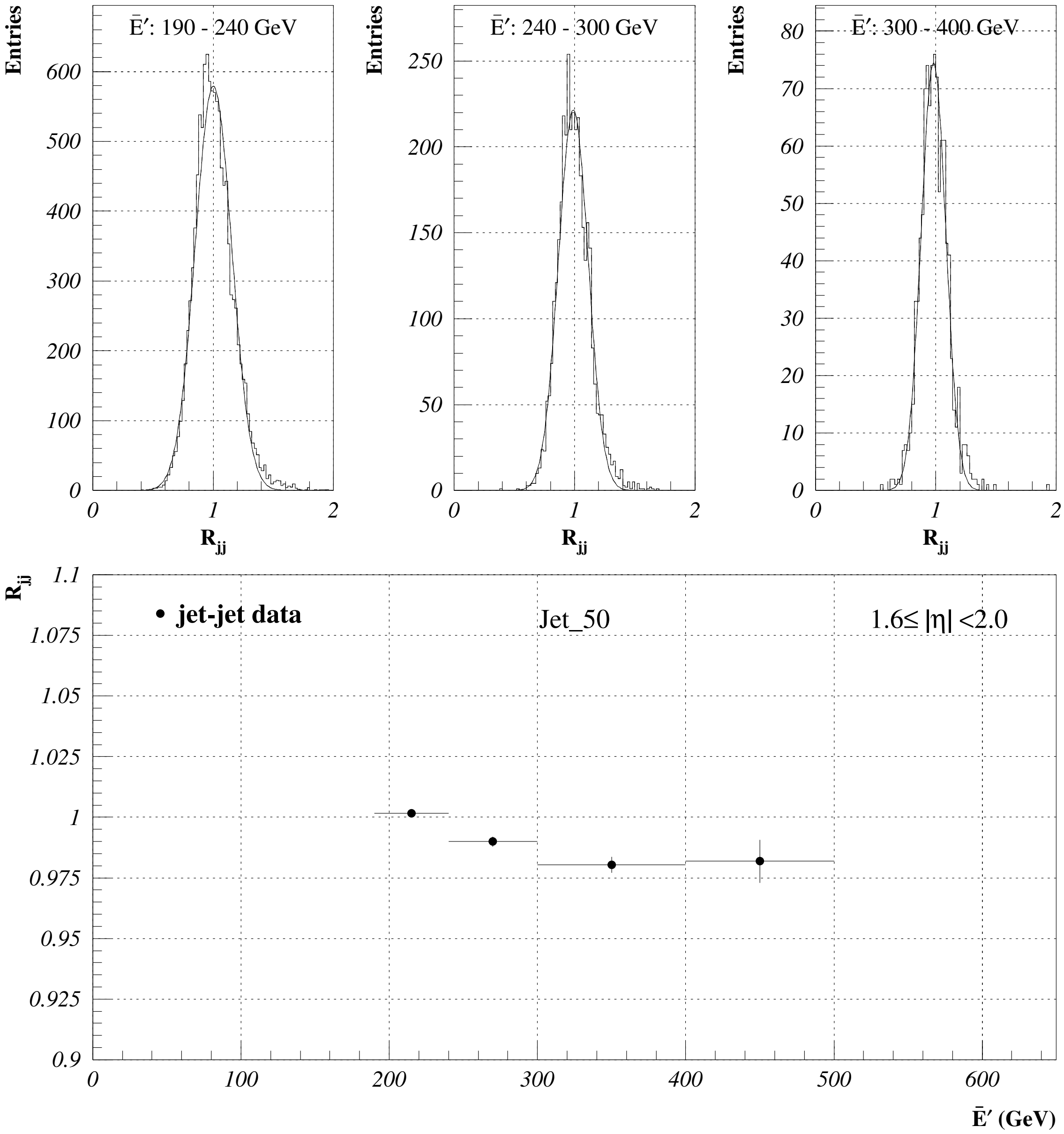

Figure 8: *Using the* Jet_50 *data the fits to Gaussians of the* $\mathcal{R}_{jj}$ *distributions in the* E' *bins with most statistical significance are shown along with* $\mathcal{R}_{jj}$ *as a function of* $\bar{E}'$.

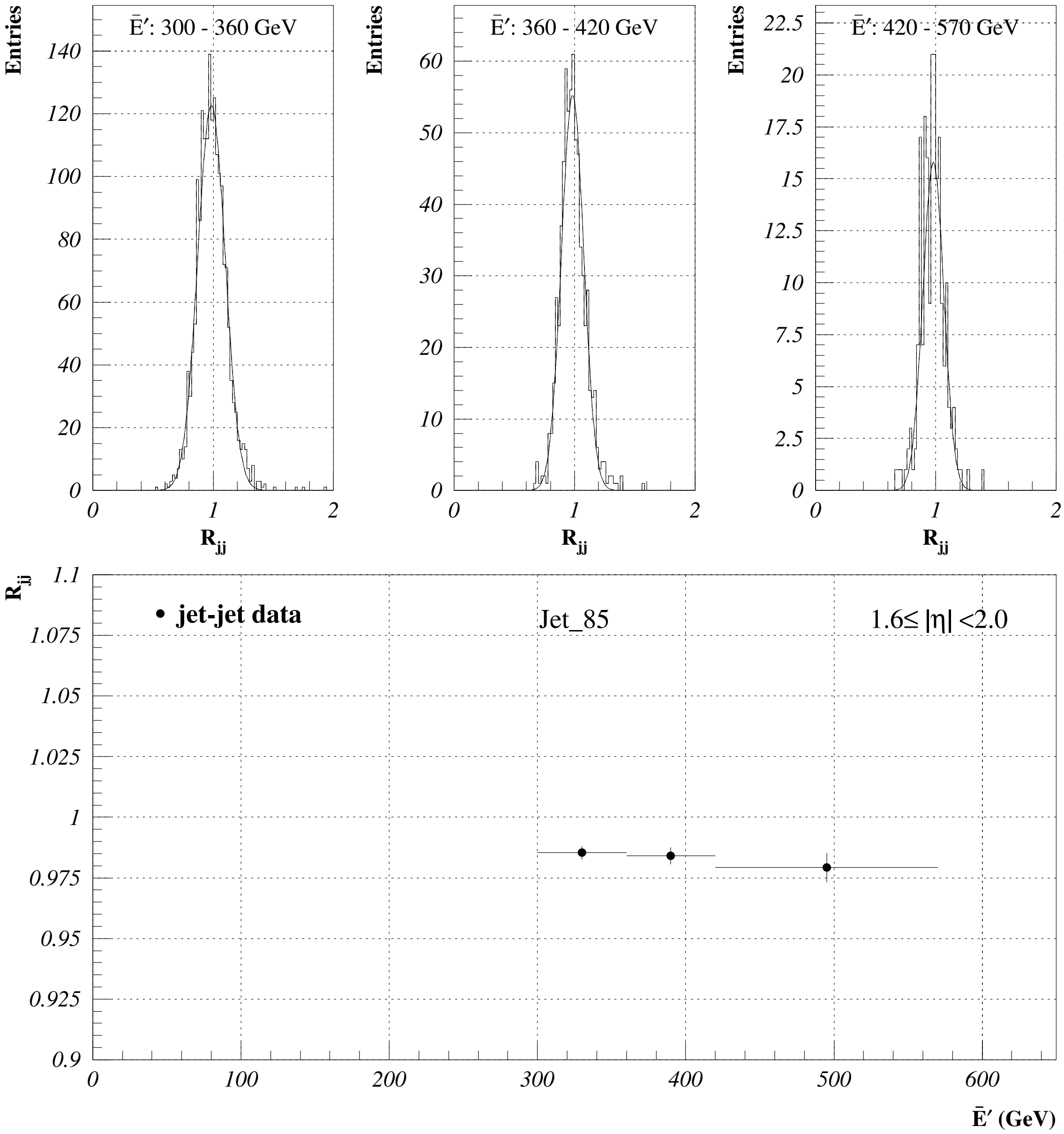

Figure 9: *Using the* Jet_85 *data the fits to Gaussians of the* $\mathcal{R}_{jj}$ *distributions in the* E' *bins with most statistical significance are shown along with* $\mathcal{R}_{jj}$ *as a function of* $\bar{E}'$.

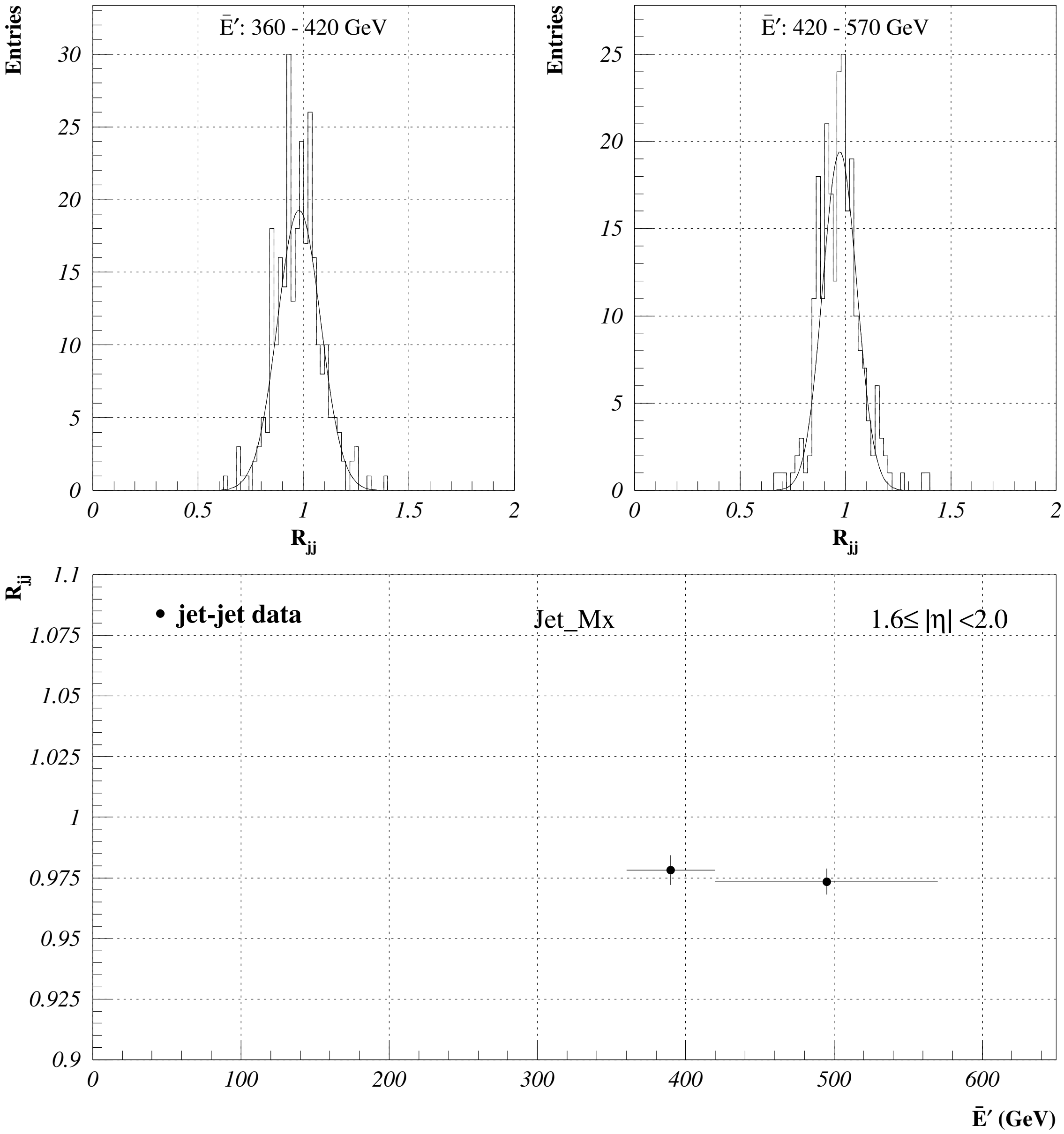

Figure 10: *Using the* Jet_Mx *data the fits to Gaussians of the* $\mathcal{R}_{jj}$ *distributions in the* E' *bins with most statistical significance are shown along with* $\mathcal{R}_{jj}$ *as a function of* $\bar{E}'$.

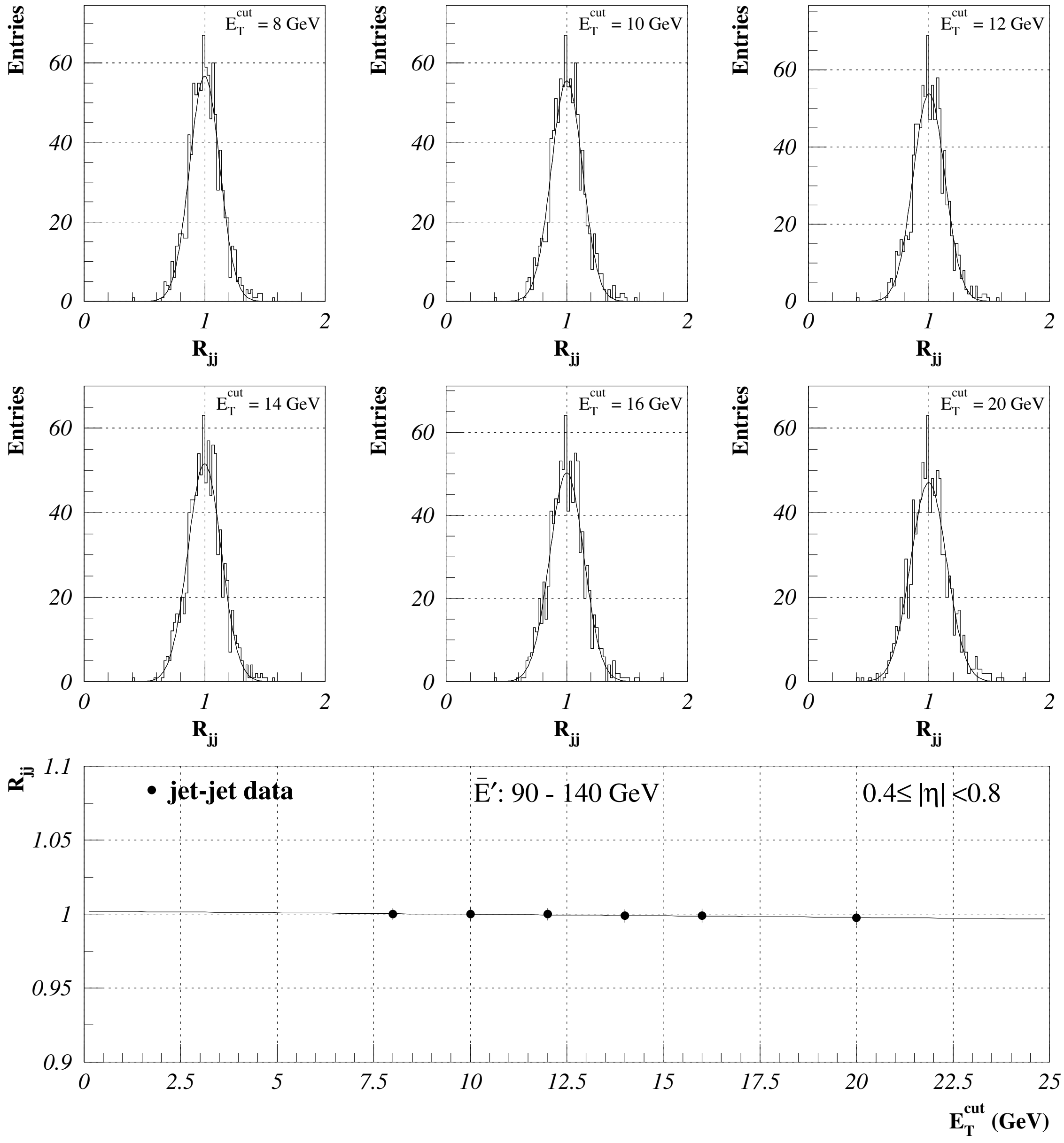

Figure 11: *Illustration of the derivation of the unclustered energy correction in jet-jet data.*

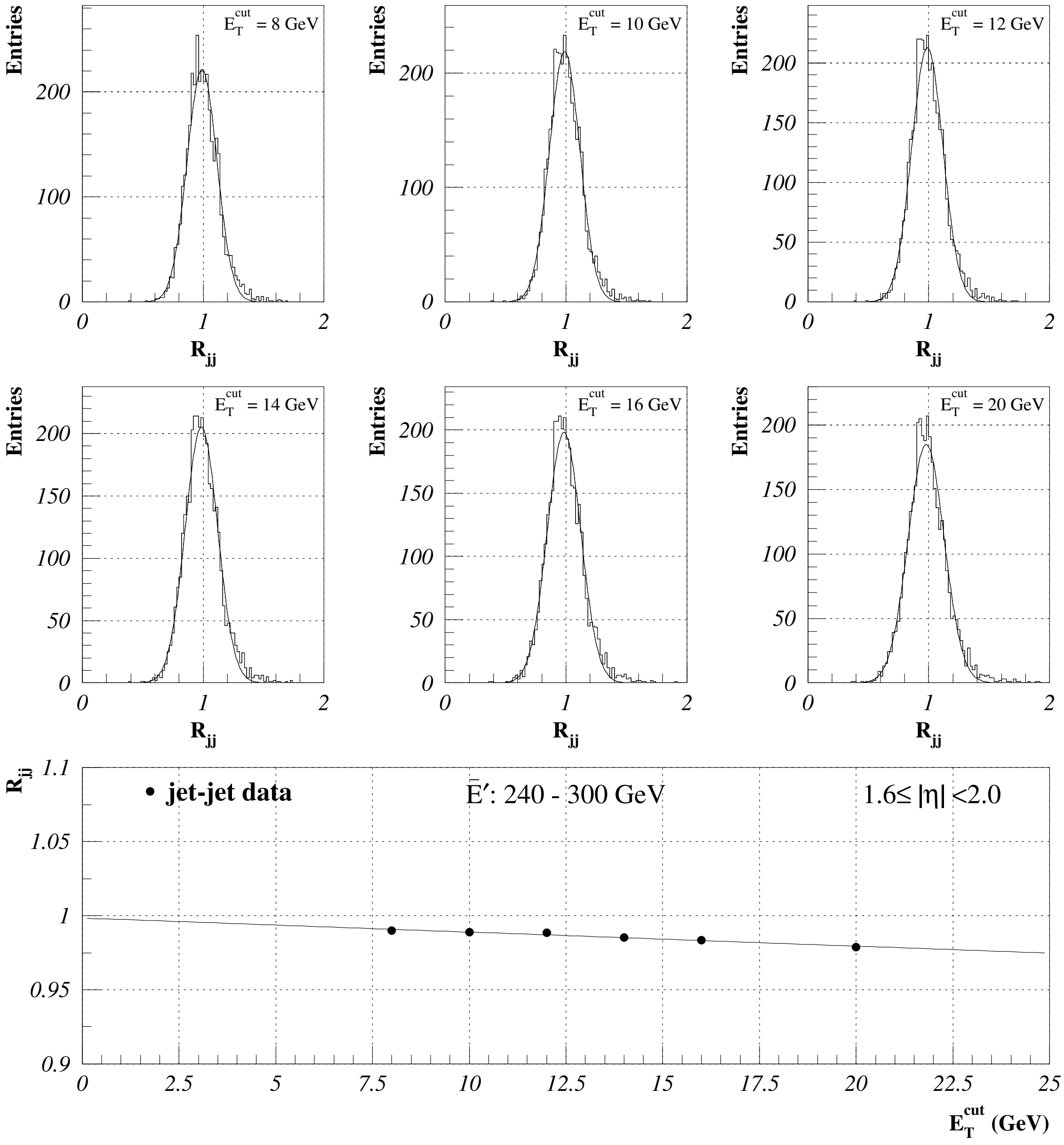

Figure 12: *Illustration of the derivation of the unclustered energy correction in jet-jet data.*